Stem Cell Reports
Article

ISSCR

OPEN ACCESS

Human Engineered Heart Tissue: Analysis of Contractile Force

Ingra Mannhardt,[1] Kaja Breckwoldt,[1] David Letuffe-Brenière,[1] Sebastian Schaaf,[1] Herbert Schulz,[2,3] Christiane Neuber,[1] Anika Benzin,[1] Tessa Werner,[1] Alexandra Eder,[1] Thomas Schulze,[1] Birgit Klampe,[1] Torsten Christ,[1] Marc N. Hirt,[1] Norbert Huebner,[2] Alessandra Moretti,[4] Thomas Eschenhagen,[1,5] and Arne Hansen[1,5,*]

[1]Department of Experimental Pharmacology and Toxicology, Cardiovascular Research Center, University Medical Center Hamburg-Eppendorf, DZHK (German Center for Cardiovascular Research), Partner Site Hamburg/Kiel/Lübeck, 20246 Hamburg, Germany
[2]Max-Delbrueck-Center for Molecular Medicine – MDC, DZHK (German Center for Cardiovascular Research), Partner Site Berlin, 13092 Berlin, Germany
[3]Cologne Center for Genomics (CCG), University of Cologne, 50931 Cologne, Germany
[4]I. Medical Department - Cardiology, Klinikum rechts der Isar – Technische Universität München, DZHK (German Centre for Cardiovascular Research), Partner Site Munich Heart Alliance, 81675 Munich, Germany
[5]Co-senior author
*Correspondence: ar.hansen@uke.de
http://dx.doi.org/10.1016/j.stemcr.2016.04.011

SUMMARY

Analyzing contractile force, the most important and best understood function of cardiomyocytes in vivo is not established in human induced pluripotent stem cell-derived cardiomyocytes (hiPSC-CM). This study describes the generation of 3D, strip-format, force-generating engineered heart tissues (EHT) from hiPSC-CM and their physiological and pharmacological properties. CM were differentiated from hiPSC by a growth factor-based three-stage protocol. EHTs were generated and analyzed histologically and functionally. HiPSC-CM in EHTs showed well-developed sarcomeric organization and alignment, and frequent mitochondria. Systematic contractility analysis (26 concentration-response curves) reveals that EHTs replicated canonical response to physiological and pharmacological regulators of inotropy, membrane- and calcium-clock mediators of pacemaking, modulators of ion-channel currents, and proarrhythmic compounds with unprecedented precision. The analysis demonstrates a high degree of similarity between hiPSC-CM in EHT format and native human heart tissue, indicating that human EHTs are useful for preclinical drug testing and disease modeling.

INTRODUCTION

The advent of human induced pluripotent stem cell (hiPSC) technology and protocols to efficiently differentiate cardiomyocytes (CM) (Burridge et al., 2012) have opened the perspective to use hiPSC-CM for cardiac research or drug development. This biotechnology advancement also boosted the development of test systems to evaluate hiPSC-CM electrophysiology (reviewed in Hoekstra et al., 2012), impedance (Guo et al., 2013; Scott et al., 2014), field potentials (Caspi et al., 2009; Harris et al., 2013; Navarrete et al., 2013; Clements and Thomas, 2014; Riedel et al., 2014; Qu and Vargas, 2015), action potentials and calcium transients with fluorescent dyes, and cellular shortening video-optically (Lee et al., 2012; Lopez-Izquierdo et al., 2014; Feaster et al., 2015; Pointon et al., 2015). These assays may improve preclinical drug development and safety toxicology, because current systems are based either on recombinant cell lines or animal cells, both susceptible to typical shortcomings. HiPSC-CM promise an intact, human cardiomyocyte context in which a drug and/or principle is tested. Moreover, patient-specific cell lines offer (1) the perspective of testing drugs in a wide spectrum of genetic backgrounds and (2) individualized risk prediction and testing of adverse drug effects. Different technologies have been employed for predictive toxicology application (Braam et al., 2010; Pointon et al., 2015), and many studies have successfully demonstrated disease-specific phenotypes in hiPSC-CM from patients with inherited cardiac diseases (reviewed in Moretti et al., 2013; Karakikes et al., 2015). Most test systems use hiPSC-CM as 2D layers on rigid plastic cell-culture dishes that do not allow the cells to perform physiological auxotonic contractions (Nishimura et al., 2004). Contractile function, the main feature of the heart, can only be analyzed in a very restricted manner.

We have developed protocols to form 3D force-generating engineered heart tissues (EHTs; Eschenhagen et al., 2012; Hirt et al., 2014). This follows the principle of hydrogel formation with dissociated cardiomyocytes in casting molds and maintenance with a defined preload. Cardiomyocytes remodel the hydrogel, align along force lines, increase in size, and form a coherently beating syncytium. Potential advantages of the EHT system for preclinical drug development and safety toxicology are 2-fold. (1) It allows monitoring effects of drugs on all major parameters of heart function: force, pacemaking activity and contraction, and relaxation kinetics. (2) The analysis is done under stable conditions that resemble cardiac physiology, i.e., 3D heart-like muscle strips that contract under auxotonic, work-performing, steady-state conditions.

First publications with EHTs from human embryonic stem cells or hiPSC-CM demonstrated the principal

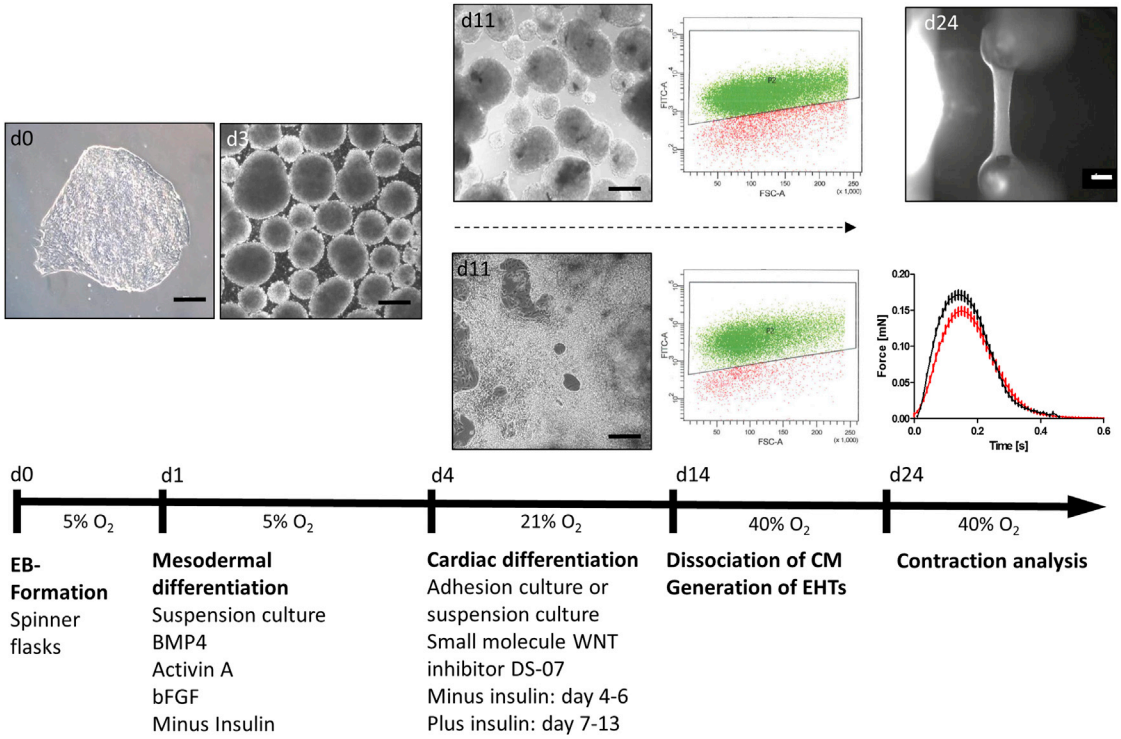

Figure 1. Cardiac Differentiation Protocol

Spontaneous beating started at days 9–11 of differentiation. Beating cells were dissociated, subjected to fluorescence-activated cell sorting analysis (cTNT), and used for EHT generation (d14; see also Movies S4 and S5). EHTs started coherent beating at days 10–14 after casting and enabled for functional analysis (see also Movie S1; scale bar, 1 mm). Average contraction peaks of spontaneously beating (black) and electrically paced EHTs (red; 1.5 Hz; 20–35 days after casting) in modified Tyrode's solution with 1.8 mM calcium are shown (n = 50 EHTs from seven independent experiments per group; depicted are mean ± SEM). Scale bars, 200 μm. See also Figure S1.

feasibility to generate human constructs and some basic characterization (Schaaf et al., 2011; Tulloch et al., 2011; Kensah et al., 2013; Nunes et al., 2013; Thavandiran et al., 2013). However, neither we nor others have yet shown that EHTs from hiPSC-CM are indeed suitable for the proposed purpose, i.e., whether they faithfully replicate effects on indicator compounds affecting rate, force, and contraction kinetics. This is particularly important for inotropes, since modulators of inotropy are a mainstay of cardiac drug development and new concepts are urgently needed (Francis et al., 2014). The present study therefore set out to answer the following questions. (1) Do drugs known to interfere with pacemaking mechanisms in the sinoatrial node (SAN) affect the spontaneous beating rate of hiPSC-EHTs? (2) Do positive and negative inotropic drugs affect contraction force of hiPSC-EHTs in a manner similar to that of human heart muscle strips? (3) Do drugs with known and supposedly specific effects on individual ion currents affect contractile function? (4) Is prolongation of relaxation time a surrogate for prolongation of repolarization and proarrhythmic risk?

RESULTS

Differentiation Results and Baseline Characterization of hiPSC-EHTs

Formation of embryoid bodies (EBs) in spinner flasks resulted in homogeneous EBs of 54 ± 1 μm (n = 198) diameter. The average differentiation efficiency was 87% ± 9% (n = 20) with an input/output ratio of 1:1.2 ± 0.8 (hiPSC/hiPSC-CM). Human EHTs started to beat spontaneously and regularly 10–14 days after casting and continued for several weeks (25- and 74-day-old EHT are shown in Movies S1 and S2). Baseline contractility parameters under auxotonic conditions (20- to 25-day-old EHTs from seven different cardiomyocyte batches; n = 75/7) were 61 ± 2 bpm (frequency), 0.152 ± 0.006 mN (force), 0.120 ± 0.002 s (T1, contraction time), 0.163 ± 0.003 s (T2, relaxation time), 1.51 ± 0.07 mN/s (maximal contraction velocity), and 1.11 ± 0.06 mN/s (maximal relaxation velocity). Average peaks of spontaneously beating and electrically paced EHTs (n = 50) are shown in Figure 1. During cardiac differentiation, expression of the pluripotency

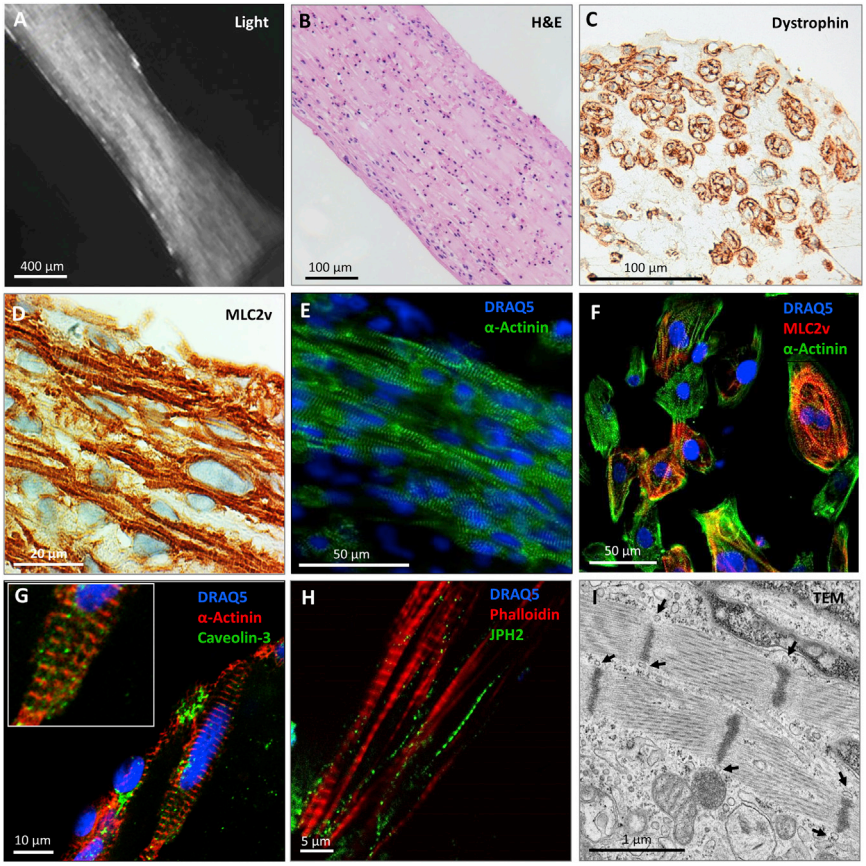

Figure 2. Histological Evaluation of hiPSC-EHTs

(A) Representative still view of a living EHT.

(B) Longitudinal section stained with H&E.

(C) Cross section stained for dystrophin.

(D) Longitudinal section stained for MLC2v.

(E) Whole-mount immunofluorescence confocal microscopic section of EHT stained with DRAQ5 (nuclei, blue) and α-actinin (green).

(F) Confocal analysis of hiPSC-CM cultured in 2D for 30 days stained with DRAQ5 (blue) and antibodies against cardiac MLC2v (red) and α-actinin (green).

(G and H) Whole-mount immunofluorescence confocal microscopic section of 30- to 35-day-old EHTs stained with DRAQ5 (blue) and antibodies against α-actinin (red; G) and caveolin-3 (green; G) or phalloidin (red; H) and an antibody against junctophilin-2 (green; H).

(I) Transmission electron microscopy of 35-day-old EHT. Arrows indicate structures resembling t tubules.

See also Figure S2.

gene *OCT-4* declined, expression of mesoderm genes (*MESP*, *VEGFR2*) increased transiently, and expression of cardiac genes increased progressively (Figure S1A). Differentiated cardiomyocytes were mainly $MLC2a^{+}/MLC2v^{-}$ and developed to an $MLC2a^{-}/MLC2v^{+}$ cardiomyocyte population in the EHT format (Figures S1B and S1C). The non-cardiomyocyte fraction at the end of differentiation was investigated by gene-expression analysis. Besides cardiac genes, the most prominently expressed genes were those typical for (myo)fibroblast-like cells, while genes for other cell types were expressed below 1% of cardiac gene expression level (Figure S1D).

Still pictures of live EHTs taken with the video camera of the EHT setup (Figure 2A and Movie S1) demonstrated macroscopically distinguishable muscle bundles in EHTs. Histological analysis of 30- to 35-day-old EHTs revealed structural anisotropy with cellular alignment in parallel to the force lines spanning along the longitudinal axis of the tissue (Figure 2B) and appearing as round, dystrophin-positive CM in cross sections (Figure 2C). CM in EHTs were characterized by regular sarcomeric organization of α-actinin and a high degree of MLC2v-positive CM (Figures 2D and 2E), whereas CM cultured in 2D showed poor sarcomeric organization and less cellular alignment (Figure 2F). Caveolin-3 immunofluorescence provided initial evidence for immature t-tubule formation by demonstrating punctual but irregular staining pattern and areas with poorly organized caveolin-3-positive structures as an indicator for developing caveolae (Figure 2G). This irregular staining pattern was also apparent in EHTs stained with an antibody against junctophilin-2 (Figure 2H). Transmission electron microscopy (TEM) confirmed orientation and alignment of sarcomeric structures with regular Z lines, and inconsistent I- and A-band formation (Figure 2I). Average sarcomere length was 1.6 ± 0.1 µm (n = 20 sarcomeres); mitochondria were frequent and exhibited mainly immature cristae-subtype with sparse cristae formation. Tubular structures (~60–80 nm diameter) were detected in close proximity to Z lines. Gene expression of ion channels and cardiac markers indicated overall similar expression in EHT and 2D (Figures S2A and S2B). Microarray analysis (Table S1; NCBI GEO accession number GEO: GSE80390) of differentiated cardiomyocytes, EHT, and 2D CM samples revealed 5,687 significantly expressed genes (false-discovery rate [FDR] <5%, Table S1). Probes below 0.1% FDR (n = 277) were further investigated using clustering (Figure S2C) and functional enrichment approaches (Table S2). Several

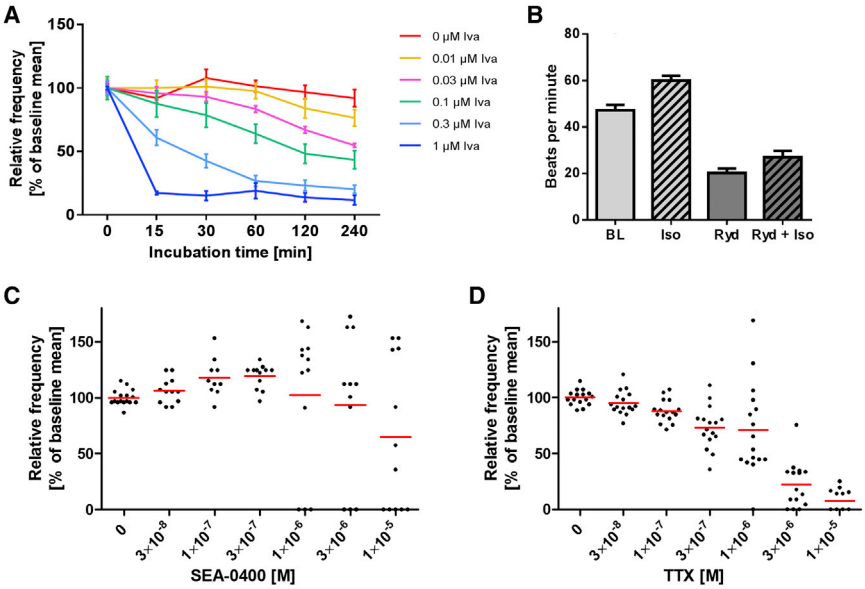

Figure 3. Modulation of Spontaneous Beating Frequency of hiPSC-EHTs in Modified Tyrode's Solution

Replicates are indicated as EHTs/number of independent experiments. Data are depicted as mean ± SEM (A and B) or scatter plots with means (C and D).

(A) Ivabradine effect at 1.8 mM calcium; n = 4/1.

(B) Effect of 100 nM isoprenaline (Iso), 10 µM ryanodine (Ryd), or isoprenaline after ryanodine preincubation (Ryd + Iso, 5 min) at 0.6 mM calcium; n = 4–8/1.

(C) Effect of SEA-0400 at 1 mM calcium (1 hr incubation time); n = 12–16/2.

(D) Effect of tetrodotoxin (TTX) at 1.8 mM calcium; n = 16/2.

See also Figure S3.

calcium-handling proteins (L-type calcium channels, LTCC; Na^+/Ca^{2+}-exchanger, NCX1; Na^+/K^+-ATPase; Na^+/H^+-exchanger, NHE1; SR Ca^{2+}-ATPase, SERCA; phospholamban [PLN]) were detected in 2D and EHT by western blot (Figure S2E).

Functional Characterization of hiPSC-EHTs

The basis for the characterization of the hiPSC-EHT model are 26 concentration-response curves (CRC), depicted as scatterplots in Figures S5–S7.

Pacemaker Mechanisms

To investigate pacemaker mechanisms in hiPSC-EHTs, we analyzed the contraction pattern by video-optical recording (Figure S3). We tested five compounds interfering relatively selectively with the membrane clock (ivabradine with hyperpolarization-activated cyclic nucleotide-gated [HCN] channels), the SR-based calcium clock (ryanodine with ryanodine receptors, SEA-0400 with NCX), or both proposed pacemaker mechanisms (isoprenaline with PLN and HCN channels) or sodium-channel activity (TTX). Ivabradine (0.01–1 µM) concentration- and time-dependently decreased spontaneous beating frequency with half-maximal effects at ~50 nM and almost complete inhibition at 1 µM (Figures 3A and S7N). Ryanodine (10 µM) decreased the spontaneous beating rate (from 47 ± 6 to 20 ± 2 bpm; n = 4) and antagonized the positive chronotropic effect of isoprenaline (Figure 3B), which itself amounted to +27% (from 47 ± 6 to 60 ± 4 bpm). The NCX inhibitor SEA-0400 induced complex responses. Some EHTs showed an increase in spontaneous beating frequency and others a reduction, and some ceased beating at high concentrations (10 µM, Figures 3C and S7O). TTX concentration-dependently decreased the beating rate with a threshold concentration of 300 nM (Figures 3D, 6B, S6B, and S6D).

Physiological Force Modulation

HiPSC-EHTs displayed a concentration-dependent positive inotropic response to increasing extracellular calcium concentrations with an half maximal effective concentration (EC_{50}) of 0.6 mM calcium (n = 8; Hill slope 1.96; Figures 4A and S5A). Under pacing, EHTs followed electrical stimulation between 1 and 2 Hz and partially lost capture above 2 Hz (Figure 4B). At pacing rates below 1 Hz, frequency-control was incomplete due to higher spontaneous beating frequency for some EHTs. An increase in beating rate between 1.0 and 2.0 Hz resulted in reduction of contraction time and relaxation time (frequency-dependent acceleration of relaxation [FDAR] −18%), but no change of contractile force (no Treppe phenomenon; Figure 4C). β-Adrenergic stimulation with isoprenaline (100 nM at 0.6 mM Ca^{2+}, 2-Hz pacing frequency) led to an increase in contractile force (+41% ± 7%; n = 13), no change in contraction time T1 (−2% ± 2%; n = 13), and a decrease in relaxation time T2 (−20% ± 4%; n = 13; Figure S5B). The positive lusitropic effect of isoprenaline was antagonized by the muscarinic agonist carbachol (10 µM, T2 +31% ± 5% compared with isoprenaline; n = 13; Figure 4D). Increasing the preload resulted in an increase in contractile force from 43% ± 5% to 100% (maximum force; n = 9). Maximum force was reached at 107% of slack length (Figure 4E). Post-rest potentiation (PRP) was analyzed in the presence of SEA-0400 (10 µM). This reduced the spontaneous beating rate and potentially aggravated the potentiation: After 200 s of pacing (1.5 Hz) a 20-s-long pacing pause was introduced before pacing was reinitiated. Comparison of the last contraction peak before and the first

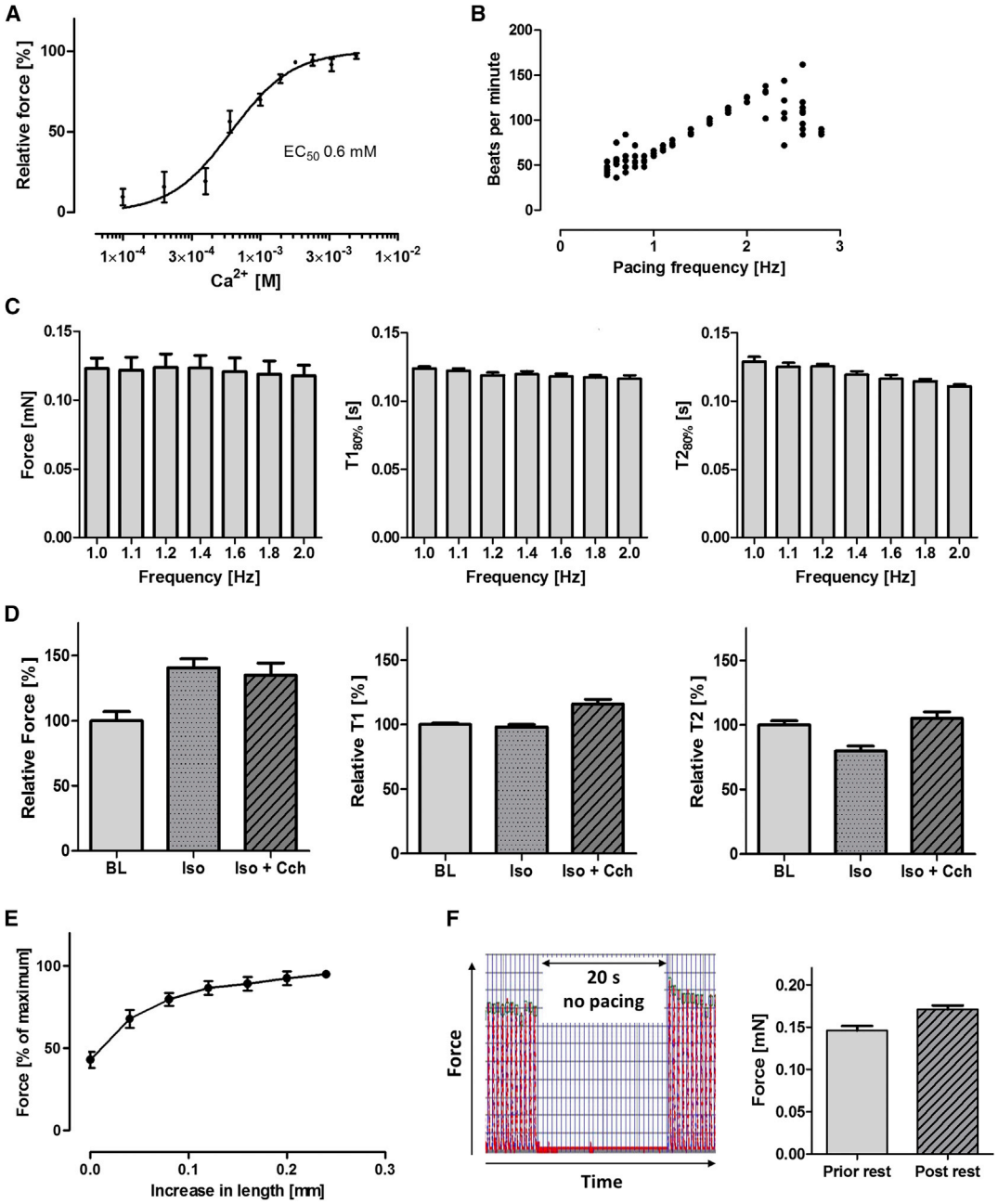

Figure 4. Regulation of Contractile Function of hiPS-EHTs by Physiological Interventions

All experiments were carried out in modified Tyrode's solution; replicates are indicated as EHTs/number of independent experiments; error bars are SEM.

(A) Calcium concentration-response curve at 2-Hz electrical stimulation (n = 8/2).

(B) Beating rate at pacing frequencies between 0.6 and 3.0 Hz (n = 8/1).

(C) Force/contraction time/relaxation time-frequency relationship at 1.0 mM external calcium (n = 8/1).

(D) Response of electrically stimulated (2 Hz) EHTs to 100 nM isoprenaline (Iso) and 10 μM carbachol (CCh) at 0.6 mM calcium (n = 13/2).

(E) Frank-Starling mechanism. Increase in force in relation to increased preload at 1.8 mM calcium and 2 Hz (n = 5–9/1).

(F) Post-rest potentiation of EHTs at 1 mM calcium in the presence of 10 μM SEA-0400. Representative example (20 s rest, pacing with 1.5 Hz) and statistical evaluation (n = 8/1).

See also Figure S4.

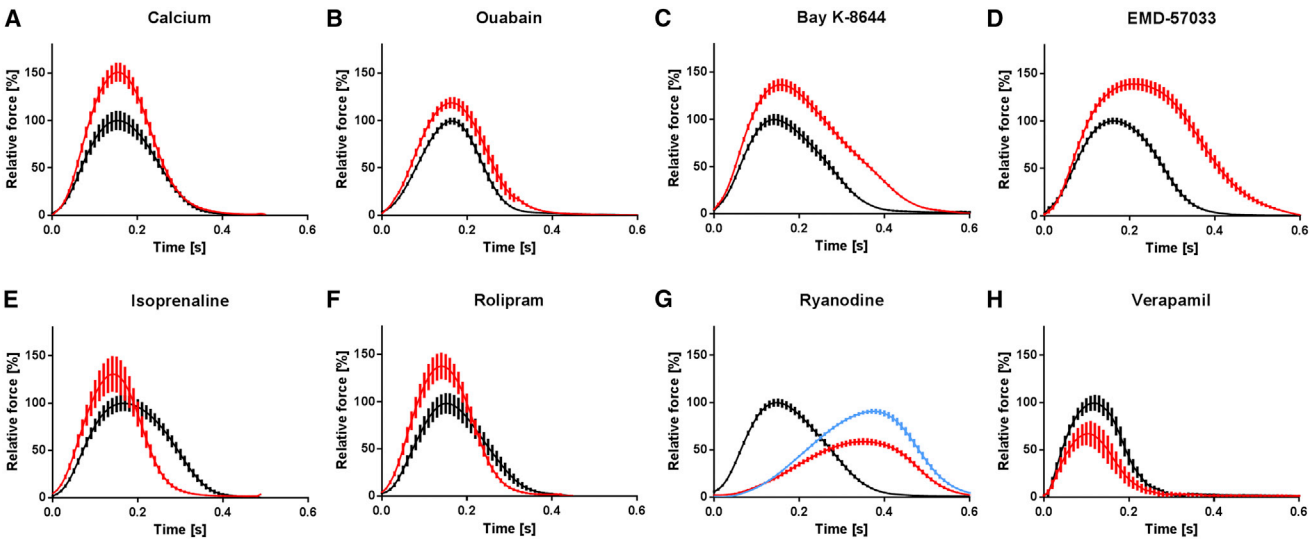

Figure 5. Regulation of Contractile Function of hiPSC-EHTs by Inotropic Drugs

Average contraction peaks before (black) and after (red) the respective inotropic drug intervention.

(A–H) Positive inotropic drugs (A–F) were tested at submaximal (0.5–0.6 mM), and negative inotropic drugs (G and H) at high (1.8 mM; H) and submaximal (0.5 mM; G) calcium concentrations. Depicted is the electrically stimulated (1.5–2 Hz) mean relative force in percentage of baseline maximum ± SEM in modified Tyrode's solution; replicates are indicated as EHTs/number of independent experiments. (A) calcium (5 mM; n = 8/2). (B) ouabain (100 nM; n = 6/2). (C) Bay K-8644 (300 nM; n = 4/1). (D) EMD-57033 (10 μM; n = 4/1). (E) isoprenaline (100 nM; n = 4/1). (F) rolipram (10 μM) + isoprenaline (100 nM, red) versus isoprenaline (100 nM, black; n = 11/2). (G) ryanodine (0.3 μM, red; 10 μM, blue; n = 6/2). (H) verapamil (1 μM; n = 18/2).

See also Figure S5.

after the pacing pause revealed a PRP of +17% (n = 11; Figure 4F). The selective inhibitor of the slowly activating delayed rectifier current I_{Ks}, HMR-1556, was tested in the presence of β-adrenergic activation and I_{Kr} inhibition, a protocol that revealed maximal contribution of I_{KS} to repolarization in human ventricular myocardium (Jost et al., 2005). HMR-1556 slightly reduced the isoprenaline-stimulated spontaneous beating rate, but failed to affect relaxation time or force, whereas E-4031 increased relaxation time by +82% in an isoprenaline-sensitive manner (n = 4/1; Figure S4).

Pharmacological Force Regulation

We analyzed the effect of positive and negative cyclic AMP (cAMP)-dependent and -independent inotropic modulators (calcium, ouabain, Bay K-8644, EMD-57033, isoprenaline, rolipram, ryanodine, and verapamil) under rate control (1–2 Hz). Average contraction peaks are depicted in Figure 5 (complete CRCs are shown in Figure S5). These peaks demonstrate canonical inotropic changes for all compounds tested, associated with characteristic changes in contraction kinetics. Ca^{2+}, ouabain, and verapamil modulated force without a change in contraction kinetics, while the increase in force development in the presence of the cAMP-dependent drugs isoprenaline and rolipram was accompanied by the typical hastening of relaxation (positive lusitropic effect). Conversely, the Ca^{2+} channel agonist Bay K-8644 and the myofilament Ca^{2+} sensitizer EMD-57033 markedly prolonged relaxation (negative lusitropic effect). Ryanodine displayed typical biphasic responses, with negative inotropic effects at low (0.3 μM) and positive inotropic effects at high (10 μM) concentrations and a pronounced increase in contraction time (T1), as shown for myocardium tissue (Sutko and Willerson, 1980).

Modulators of the Cardiac Ion Channels

Antagonists and agonists of ion channels were analyzed in spontaneously beating EHTs (Figures 6 and S6). Delayed inactivation of the fast sodium current I_{Na} by ATX-II or activation of the L-type calcium current $I_{Ca,L}$ by Bay K-8644 prolonged relaxation time T2 as did E-4031, a selective inhibitor of the repolarizing, rapidly activating delayed rectifier current I_{Kr}. ATX-II had the most pronounced effect (556% ± 31% of baseline; see also Movie S3), Bay K-8644 mainly inhibited early relaxation, and E-4031 induced typical after-contractions. Conversely, NS-1643, an agonist of I_{Kr}, concentration-dependently reduced T2, which was accompanied by increased spontaneous beating frequency and an increase in contractile force. At high concentrations (0.1 mM) EHTs demonstrated an irregular beating pattern, indicated by high scatter for all contractility parameters (Figures 6D and S6G). TTX slowed the spontaneous beating rate as seen before (Figure 3D), but did not have a major effect on force or contraction kinetics (Figure S6D). The $I_{Ca,L}$

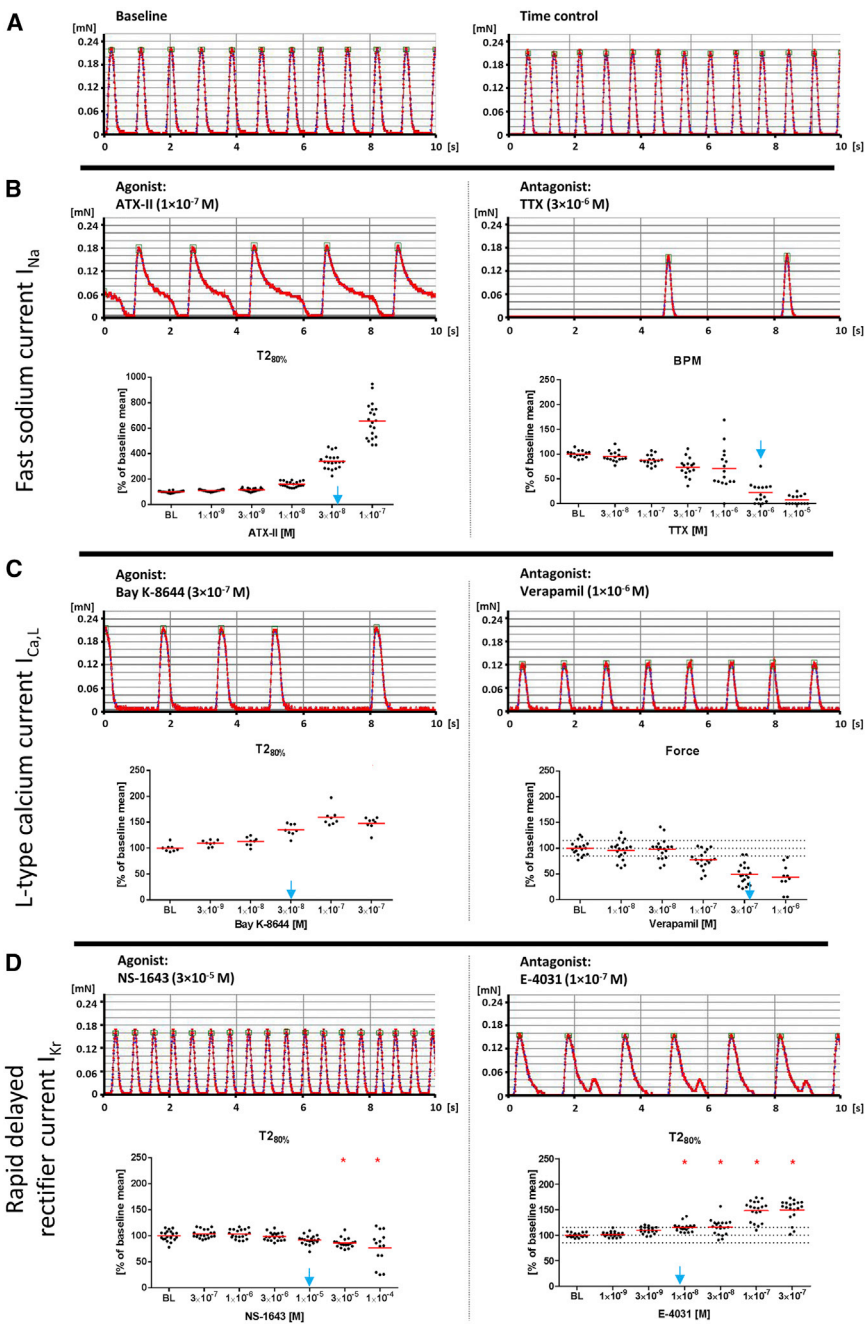

Figure 6. Effect of Specific Ion-Channel Modulators on Spontaneous Contractions of hiPSC-EHTs

Data are depicted as single values and mean; replicates are indicated as EHTs/number of independent experiments.

(A) Regular spontaneous beating pattern under baseline condition (left) and 3 hr later (time control, right).

(B–D) Concentration-response curves (B) Left: ATX-II (I_{Na} gating inhibitor, agonist; n = 20/2); right: TTX (I_{Na} antagonist; n = 16/2). (C) Left: Bay K-8644 ($I_{Ca,L}$ agonist; n = 8/2); right: verapamil ($I_{Ca,L}$ antagonist; n = 19/2). (D) Left: NS-1643 (I_{Kr} agonist; n = 20/3); right: E−4031 (I_{Kr} antagonist; n = 20/3). Depicted are representative original recordings and concentration-response curve for the most sensitive contraction parameter (T2, relaxation time at 80% relaxation, BPM, beats per minute). Blue arrows indicate published EC_{50}/IC_{50} values (Oliveira et al., 2004; Kaufmann et al., 2013; Bechem and Schramm, 1987; Ferry et al., 1985; Casis et al., 2006; Zhou et al., 1998). Statistical analysis was conducted by one-way ANOVA with Dunnett's post test versus baseline conditions (BL) for experiments with ≥ 3 independent experiments; *p < 0.05.

See also Figure S6.

antagonist verapamil concentration-dependently decreased contractile force (as seen before under electrical pacing, Figure 5H) and had only slight effects on contraction kinetics (Figure S6F). The expression of the respective ion channels was verified as stated above (Figure S2). To examine the compatibility of this protocol with cardiomyocytes from commercial sources, we also generated EHTs with Cor.4U and iCell CM. Figure S6A shows spontaneous and electrically stimulated average contraction peaks of Cor.4U and iCell EHTs compared with the in-house reference cell line differentiated with the protocol described herein. The EHTs from these commercial cell lines responded similarly to the aforementioned ion-channel modulators (Figure S6B).

Proarrhythmic Compounds

Drug-induced increase in action potential duration (APD_{90}) is an important indicator for proarrhythmic cardiotoxicity (Redfern et al., 2003). The results with the ion-channel model compounds ATX-II, Bay K-8644, and E-4031 indicated that relaxation time T2 of hiPSC-EHTs

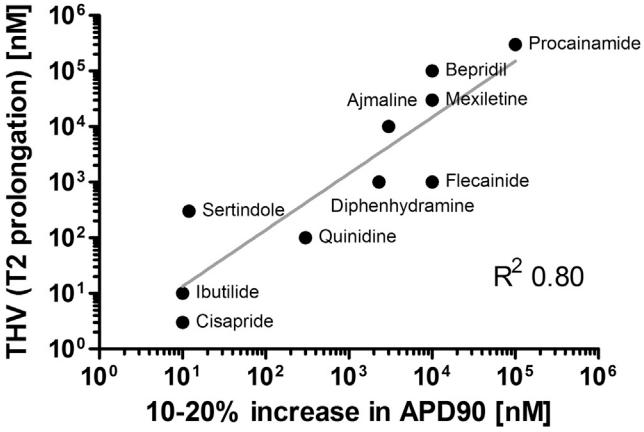

Figure 7. Correlation Analysis

Correlation between threshold value (THV) for prolongation of relaxation time (T2, EHT) and increase in APD_{90} (10%–20%, Redfern et al., 2003), Pearson correlation $R^2 = 0.80$. See also Figure S7.

might be a suitable surrogate parameter for repolarizing time or APD_{90}. We therefore determined the effect of ten known proarrhythmic compounds and, in line with the often complex, nonselective actions of these compounds, observed concentration-dependent effects on spontaneous beating frequency, force, and T2 (Figures S7A–S7J). We plotted threshold values of T2 prolongation against published concentrations of these compounds, increasing ADP_{90} by 10%–20% (Figure 7; Redfern et al., 2003). This analysis demonstrates a very strong correlation between these two parameters (correlation coefficient $R^2 = 0.80$). On the other hand, cardio-safe drugs (verapamil, ampicillin, paracetamol, aspirin; Figures S6F and S7K–S7M) did not affect T2 in this model.

DISCUSSION

In this study we evaluated the morphology and function of engineered 3D heart muscle strips (EHTs) from hiPSC-CM and their suitability for drug screening. The protocol allows analysis of contractile force with high levels of automation but requires 1×10^6 cells per EHT and 14 days of incubation time after casting. Our main findings are as follows. (1) The EHT format supports excellent heart muscle formation and morphological maturation of hiPSC-CM. (2) Modulation of beating frequency by isoprenaline, ivabradine, ryanodine, SEA-0400, and TTX suggests both calcium- and membrane-clock mechanisms to be involved in spontaneous pacemaking of hiPSC-CM/EHTs and an overall similarity with newborn SAN pacemaking. (3) Human iPSC-EHTs exhibited a positive force-length relationship and FDAR and PRP, but a neutral force-frequency relationship. (4) Canonical responses to cAMP-dependent and -independent positive and negative inotropic drugs were observed. (5) There was high sensitivity and specificity for selective ion-channel modulators; several proarrhythmic and safe drugs make hiPSC-EHT a promising model for preclinical drug screening.

Less than a decade after the establishment of the first protocol for the generation of hiPSC (Takahashi et al., 2007), CM can now be differentiated from hiPSC at high efficiency and are commercially available. Thus, hiPSC-CM are increasingly used for biomedical applications and have a chance to partially replace the mouse, with its known limitations, as the standard model in cardiovascular research. Yet the true value of hiPSC remains controversial, in part because of limited functional readout assays. Our study addressed these issues and tried to answer via a systematic approach to what extent the automated 24-well hiPSC-EHT assay is suitable as a robust, high-content contractile force assay.

The experimental design of this model provides several differences to standard 2D culture: EHTs are anchored between two flexible silicone posts, which generate a preload, and EHTs perform auxotonic contractile work (the physiological form of cardiac contraction) against elastic posts. This results in macroscopically distinguishable muscle bundles, a high degree of CM alignment and orientation, good sarcomeric organization, and cross-striated CM approaching the classical rod shape of adult ventricular myocytes. These results compare favorably with human embryonic stem cell- and hiPSC-CM cultured in classical monolayers that are polymorphic and small, isotropically oriented, and have disarrayed sarcomeres and very immature ultrastructural organization (reviewed in Yang et al., 2014). Furthermore, TEM, confocal immunofluorescence microscopy, and western blot analysis revealed that CM in EHTs have a relatively high mitochondrial density and express classical calcium-handling proteins. TEM and staining for caveolin and junctophilin are compatible with nascent t tubules, but the data clearly do not qualify as proof of an established t-tubular system in hiPSC-CM in EHTs. Others have shown that culture time is important for the structural and functional development of hiPSC-CM in 2D (Lundy et al., 2013) and that 1-year-old CM cultured at very low density exhibits increased size, longer and better organized sarcomeres, greater transcript levels of cardiac marker proteins, longer action potentials, and signs of metabolic switch that could be mimicked by overexpressing the microRNA let-7 (Kuppusamy et al., 2015). Since EHTs are cultured for only 2–3 weeks before the first measurements, other factors such as the 3D heart muscle-like environment and load likely participate in this development process. The impact of load on cardiomyocyte development is also supported by a recent study in neonatal rat EHTs demonstrating that increasing the load

by inserting metal braces induced a phenotype of pathological cardiac hypertrophy in rat EHTs (Hirt et al., 2012), indicating that culture under isometric conditions (stiff posts or 2D cultures on plastic surfaces) may in fact induce a pathological phenotype. Somewhat surprisingly, EHTs could readily be generated not only from hiPSC-CM preparations with 60%–90% purity, but also from two commercially available hiPSC-CM (CDI, Axiogenesis), which, by genetic selection, are essentially free of non-myocytes, suggesting that previous findings of a mandatory requirement of 25% non-cardiomyocytes in collagen-based EHTs (Naito et al., 2006) do not apply for human tissues generated with fibrin.

Contractile force in CM is the result of a fine-tuned interplay between electrical activation, calcium handling, and myofilament activation. To obtain a comprehensive picture of inotropic regulation in hiPSC-EHT, we analyzed the effects of eight compounds (calcium, ouabain, Bay K-8644, EMD-57033, isoprenaline, rolipram, ryanodine, and verapamil) that modulate contractile function by different modes of action. The data suggest that the hiPSC-EHT model replicates characteristic effects on inotropy and kinetics of contraction. The level of precision in replicating inotropic effects in hiPSC-EHTs is, to the best of our knowledge, unmatched by other approaches. For example, edge detection in 2D hiPSC-CM demonstrated high sensitivity and specificity in detecting modulators of inotropy, but failed to discriminate positive from negative inotropic agents (Pointon et al., 2015). The positive inotropic effects described in our study are smaller than in human non-failing heart tissue (Figure S5F). These differences are likely related to a lack of full maturation of CM in hiPSC-EHTs: Mitochondrial density and substructure, sarcomeric organization, intercellular connections, and t tubules are still clearly less developed in hiPSC-CM in EHTs than in native heart tissue. EHTs beat spontaneously, regulation of contractile function by physiological interventions was smaller, and a force-frequency relationship was absent. A key prerequisite for inotropic responses of CM is the precise spatial configuration of t tubules and sarcoplasmic reticulum. Even though PRP indicated functional sarcoplasmic reticulum and TEM analysis/caveolin-3/junctophilin-2 immunofluorescence suggests tubular structures in close proximity to Z lines, the irregularity and the small size indicate a very immature t-tubule/SR system. In native myocytes, the t-tubule microarchitecture is highly organized with distances to the SR of 12–15 nm. Small deviations of the spatial distance have been associated with altered calcium-induced calcium-release mechanism (Gómez et al., 1997). The much greater abnormalities of the t-tubule/SR organization in hiPSC-CM would also be compatible with the lack of a force-frequency relationship. Along the same lines, detubulation of rat myocytes by formamide-induced osmotic shock was associated with prolonged contraction peaks and calcium transients, and lack of a positive force-frequency relationship, but a preserved FDAR, positive force-calcium relationship, and positive PRP (Ferrantini et al., 2014). A study comparing human ventricular heart tissue of newborns (<2 weeks) and infants (3–15 months) observed t tubules, positive force-frequency relationship, and FDAR in infants, but only FDAR in newborns (Wiegerinck et al., 2009). PRP is directly related to the capacity of the SR to store and release calcium. The small PRP in hiPSC-EHTs suggest that the SR is incompletely developed, but functional. The link between small PRP and immaturity is also supported by a previous study demonstrating an increase in PRP with rabbit cardiomyocyte maturation between postnatal days 1–4, 14–21, and >180 (Boucek et al., 1987). On the other hand, while non-failing human heart tissue has been mainly evaluated under isometric conditions, force in hiPSC-EHTs is measured under physiological auxotonic conditions. The impact of this difference is not well characterized, but one study demonstrated 50% lower forces for auxotonic versus isometric conditions in adult rat ventricular CM (Nishimura et al., 2004).

Pacemaking in SAN cells is a complex process, explained by a combination of ion fluxes across the sarcolemmal membrane and the SR, designated as the calcium and membrane clocks (Lakatta et al., 2010). The mechanisms of spontaneous beating in hiPSC-CM are not well understood. Previous studies identified I_f current in hiPSC-CM (Ma et al., 2011). The marked efficacy and potency (EC_{50} $\sim$ 50 nM) of the I_f inhibitor ivabradine to reduce the beating rate in our study provide evidence for a major role of this current and, therefore, the membrane clock, for pacemaking in hiPSC-EHTs. Both potency and efficacy of ivabradine to decrease the beating rate in hiPSC-EHTs were much greater than in spontaneously beating right atria/SAN preparations of adult wild-type mice examined under similar conditions (Mesirca et al., 2014; no effect at 50 nM, 50% reduction at 1,000 nM). The data mirror results of genetic deletion of HCN4 in mice, which was embryonically lethal (Stieber et al., 2003), indicating a greater role of I_f for pacemaking in the developing heart. On the other hand, the effect of isoprenaline, acting by stimulating both the cAMP-sensitive I_f and Ca^{2+} uptake into the SR, was smaller in hiPSC-EHTs than in native SAN preparations (+30% versus +50% in mice; Mesirca et al., 2014). The isoprenaline effect was blocked by ryanodine at a high concentration (10 μM), suggesting that regulation of SR Ca^{2+} loading plays a major role in the isoprenaline-induced tachycardia in this model. Ryanodine itself reduced spontaneous beating frequency by 50%, similar to data in the intact canine SAN (Joung et al., 2009). Together with the rate-reducing effect of the NCX blocker SEA-0400 at

10 μM, the data suggest that both calcium- and membrane-clock mechanisms contribute to pacemaking in hiPSC-EHTs and that membrane regulation by I_f is involved in these cells. The contribution of I_f is in line with previous electrophysiological characterization of hiPSC-CM (Ma et al., 2011), but has not been observed in another hiPSC-CM model (Zhang et al., 2015). Reasons for the difference are unknown, but the clear concentration and time dependence and low half maximal inhibitory concentration (IC_{50}) of ivabradine in our experiments provide strong evidence for a specific effect. A suppression of spontaneous beating was also observed in the presence of TTX (1 μM). While TTX-sensitive sodium currents are not assumed to play a role in pacemaking in the adult SAN, 50% of newborn rabbit SAN cells express TTX-sensitive sodium currents, and this fraction decreased to 10% in adult animals (Baruscotti et al., 1996). These data suggest that pacemaking mechanisms in hiPSC-CM/EHTs resemble that of newborn SAN cells.

Modulation of cardiac repolarization is a sensitive issue in drug development, and analyses of drug effects on one of the main repolarizing currents, I_{Kr}, assayed in human ether-a-go-go-related gene (hERG)-expressing cell lines, are mandatory (Kramer et al., 2013; Okada et al., 2015). EHTs are not well suited for the determination of action potentials (e.g., with sharp microelectrodes), but offer simple and robust measurements of contraction kinetics under steady-state conditions. We therefore tested the hypothesis that drug effects on cardiac repolarization of hiPSC-EHTs can be detected by affections of the relaxation time T2 as previously demonstrated in rat EHTs (Eder et al., 2014). Indeed, stimulators (i.e., inhibitors of inactivation) of the depolarizing fast sodium current I_{Na} (ATX-II), activators of L-type calcium current $I_{Ca,L}$ (Bay K-8644), and inhibitors of the repolarizing rapidly activating delayed rectifier current I_{Kr} (E-4031) concentration-dependently prolonged T2, while activation of I_{Kr} with NS-1643 abbreviated T2. Threshold concentrations matched well with published IC_{50} or EC_{50} values on the respective channels (Figure 6). The Bay K-8644-mediated prolongation of relaxation time in spontaneously beating hiPSC-EHTs is in line with previous electrophysiological findings in hiPSC-CM, which revealed an atypical response to Bay K-8644 with a blunted increase in L-type calcium current amplitude and prolonged activation and inactivation kinetics (Kang et al., 2012; Ji et al., 2014). Effects of I_{Ks} current inhibition could not be demonstrated in hiPSC-EHT even under adrenergic stimulation and I_{Kr} block. This is in line with previous studies reporting small I_{Ks} currents of 0.31 pA/pF in 5 out of 16 analyzed hiPSC-CM (Ma et al., 2011) and insensitivity of hiPSC-CMs to I_{Ks} current inhibition in multi-electrode arrays under blinded conditions (Qu and Vargas, 2015). The data collectively indicate that I_{Ks} contributes only little to repolarization of hiPSC-CM. Taken together, the experiments with model compounds show high sensitivity of hiPSC-EHTs in detecting the effects of ion-channel modulators as alteration in T2. I_{Ks} is a notable exception.

Obviously, T2 changes are not specific for certain alterations in ion current, as modulators with different modes of action (ATX-II, Bay K-8644, E-4031) all result in similar changes. Moreover, relaxation time was also prolonged by EMD-57033, a relatively pure calcium sensitizer that prolongs relaxation by its direct effect on the myofilaments, and relaxation time was shortened by the cAMP-dependent drugs isoprenaline and rolipram, acting via phosphorylation of PLN and several myofilament proteins (Figure 5). Interestingly, neither verapamil nor TTX affected relaxation time. Their effect was visible as a concentration-dependent decrease in force and rate, respectively. The lack of verapamil effects on T2 is important for two reasons. (1) It is consistent with the effect of varying extracellular Ca^{2+} concentrations, strongly affecting peak force but not contraction kinetics. (2) Verapamil blocks I_{Kr} in addition to $I_{Ca,L}$ and is a classic example of a drug that would have failed in hERG assays, but has never been associated with proarrhythmic effects or QT prolongation. The lack of a T2 signal in hiPSC-EHTs is in line with clinical safety. Thus, the hiPSC-EHT system offers a high-content readout of contractile function, which integrates effects on depolarizing and repolarizing ion currents, myofilaments, and SR-based Ca^{2+} cycling without directly indicating the respective mechanism of action.

It seems, therefore, that this system is well suited for an initial screening of cardiac effects of drugs. The ability to detect the effects of ion-channel modulators was further challenged with a set of (previously) approved drugs, classified for their different potential to induce torsades-de-pointes arrhythmia (Redfern et al., 2003). The correlation depicted in Figure 7 demonstrates that prolongation of T2 in hiPSC-EHTs is a sensitive surrogate for APD_{90} prolongation. Given the key role of APD prolongation in drug-induced cardiac proarrhythmia (Fermini et al., 2015), a surrogate for APD prolongation might address an important aspect of in vitro cardiac safety assessment. This conclusion is strengthened by the lack of T2 effects of four compounds known to be safe (aspirin, paracetamol, ampicillin, and verapamil).

In conclusion, this study analyzes the contractile force of hiPSC-CM in the hiPSC-EHT model. Characteristic changes in contractile force are described for several physiological and pharmacological assays replicating findings of ex vivo non-failing human heart tissue, suggesting a high versatility of the hiPSC-EHT model as in vitro test system.

EXPERIMENTAL PROCEDURES

Generation of Human Engineered Heart Tissue

Spontaneously beating cardiomyocytes (day 14 of differentiation culture; Movies S4 and S5) were washed twice with PBS and digested with collagenase II (Worthington, LS004176; 200 U/ml Ca^{2+}-free HBSS [Gibco, 14175-053] with 1 mM HEPES [pH 7.4], 10 μM Y-27632, and 30 μM N-benzyl-p-toluene sulfonamide [TCI, B3082]) for 3.5 hr at 37°C (5% CO_2, 21% O_2). The dissociated cells were washed (Ca^{2+}-containing DMEM [Biochrom, F0415] with DNase [12 μg/ml; Sigma-Aldrich, D8764]; centrifugation at 100 × *g* for 15 min) and resuspended in basic medium (Ca^{2+}-containing DMEM with 1% penicillin/streptomycin). Cell count was determined (CASY) and cell concentration adjusted to 10–15 × 10^6 cells/ml. For determination of differentiation efficiency, 2 × 10^5 cells were subjected to fluorescence-activated cell sorting analysis with the directly labeled cTNT antibody (Miltenyi, 130-106-745; 1:10). Fibrin-based human EHTs were generated in agarose casting molds with solid silicone racks as previously described (Hansen et al., 2010; Schaaf et al., 2014). In brief, casting molds were generated with agarose (2% in PBS [Invitrogen, 15510-019]) and custom-made Teflon spacers in 24-well plates (Nunc, 122475). Custom-made silicone racks were placed on the 24-well plates. Cells (final concentration 10 × 10^6 cells/ml) were mixed with 100 μl/ml Matrigel (BD Bioscience, 256235), 5 mg/ml bovine fibrinogen (200 mg/ml in NaCl 0.9% [Sigma, F4753] plus 0.5 μg/mg aprotinin [Sigma, A1153]), and 2× DMEM (matching the volume of fibrinogen and thrombin for isotonization), and EHTs were generated with 100 μl per EHT (1 × 10^6 cells), 10 μM Y-27632, and 3 U/ml thrombin (100 U/ml [Biopur, BP11101104]). The cell mix was pipetted into agarose casting molds around silicone posts. After fibrin polymerization (37°C, 2 hr) the silicone racks with attached fibrin gels were transferred to new 24-well plates and cultured for 4–6 weeks (37°C, 40% O_2, 7% CO_2). The culture medium consisted of DMEM, 1% penicillin/streptomycin, 10% horse serum (Gibco, 26050), 10 μg/ml insulin, and 33 μg/ml aprotinin. Culture medium was changed on Mondays, Wednesdays, and Fridays. After 10–14 days in culture, human EHTs displayed spontaneous coherent, regular beating deflecting the silicone posts, and allowed video-optical contraction analysis. Commercial hiPSC-CM (CDI, iCell; Axiogenesis, Cor.4U) were used for comparison. Cells were thawed or dissociated according to instruction manuals, and cells counted (CASY) and EHTs prepared as stated above.

Contractile Analysis of Human EHTs

Contractile analysis was performed on 20–40-day-old EHTs in modified Tyrode's solution (120 mM NaCl, 5.4 mM KCl, 1 mM $MgCl_2$, 0.1–5 mM $CaCl_2$, 0.4 mM NaH_2PO_4, 22.6 mM $NaHCO_3$, 5 mM glucose, 0.05 mM Na_2EDTA, and 25 mM HEPES) pre-equilibrated overnight (37°C, 7% CO_2, 40% O_2). Analysis of contractile force was performed by video-optical recording as previously described (Hansen et al., 2010; Schaaf et al., 2011; Figure S1) on a setup available from EHT Technologies. When indicated, EHTs were electrically stimulated (2 V, 0.5–5 Hz, impulse duration 4 ms) with carbon electrodes as previously described using a Grass S88X stimulator (Hirt et al., 2014). The contraction peaks were analyzed in terms of frequency, force, and contraction (T1) and relaxation time (T2) at 80% of peak height (Figure S3).

Statistical Analysis

According to journal guidelines, statistical analyses were only performed (GraphPad Prism software 5.0) for experiments with ≥3 independent experiments (EHTs from ≥3 independent cardiomyocyte differentiations). Data are expressed as mean ± SEM in bar graphs (except Figure S2: mean ± SD) and curves, or as single values and mean in scatterplots. Data in the text are expressed as mean ± SD. Differences between groups were analyzed by one-way ANOVA followed by Dunnett's (all compared with baseline) post hoc multiple comparisons. Results were considered statistically significant (*) if the p value was less than 0.05. Average contraction peaks were generated from at least ten contraction peaks of several EHTs as indicated in the respective replicate number. These are depicted as mean ± SEM.

SUPPLEMENTAL INFORMATION

Supplemental Information includes Supplemental Experimental Procedures, seven figures, two tables, and five movies and can be found with this article online at http://dx.doi.org/10.1016/j.stemcr.2016.04.011.

AUTHOR CONTRIBUTIONS

I.M., T.E., and A.H. conceived and organized the project and wrote the manuscript; I.M., K.B., D.L.-B., S.S., H.S., C.N., A.B., T.W., A.E., T.S., B.K., M.H., A.M., N.H., and T.C. contributed to experiments and data analysis. All authors discussed the results and commented on the manuscript.

ACKNOWLEDGMENTS

We thank Lisa Krämer, Giulia Mearini, June Uebeler, Maksymilian Prondzynski, Sari Panjaitan, Bärbel Ulmer, Umber Saleem, Sandra Laufer, and Aya Shibamiya (HEXT Stem Cell Core Facility, UKE Hamburg) for their support. We greatly appreciate the assistance of Kristin Hartmann and Susanne Krasemann (HEXT Mouse Pathology Core Facility, UKE Hamburg), in processing histological and TEM samples. This study was supported by Deutsche Forschungsgemeinschaft (DFG Es 88/12-1, DFG Ha 3/1), the British National Centre for the Replacement Refinement & Reduction of Animals in Research (NC3Rs CRACK-IT grant 35911-259146), the European Research Council (ERC-AG IndivuHeart), the EU (FP7 Biodesign), the German Centre for Cardiovascular Research (DZHK), and the German Ministry of Education and Research (BMBF), British Heart Foundation RM/13/30157, the German Heart Foundation, the Freie und Hansestadt Hamburg, and EraNet E-RARE (01GM1305). I.M., A.E., M.H., T.E., and A.H. are co-founders of EHT Technologies GmbH, Hamburg.

Received: December 9, 2015
Revised: April 20, 2016
Accepted: April 22, 2016
Published: May 19, 2016

REFERENCES

Baruscotti, M., DiFrancesco, D., and Robinson, R.B. (1996). A TTX-sensitive inward sodium current contributes to spontaneous activity in newborn rabbit sino-atrial node cells. J. Physiol. *492*, 21–30.

Bechem, M., and Schramm, M. (1987). Calcium-agonists. J. Mol. Cell. Cardiol. *19* (*Suppl 2*), 63–75.

Boucek, R.J., Citak, M., Graham, T.P., and Artman, M. (1987). Effects of postnatal maturation on postrest potentiation in isolated rabbit atria. Pediatr. Res. *22*, 524–530.

Braam, S.R., Tertoolen, L., van de Stolpe, A., Meyer, T., Passier, R., and Mummery, C.L. (2010). Prediction of drug-induced cardiotoxicity using human embryonic stem cell-derived cardiomyocytes. Stem Cell Res. *4*, 107–116.

Burridge, P.W., Keller, G., Gold, J.D., and Wu, J.C. (2012). Production of de novo cardiomyocytes: human pluripotent stem cell differentiation and direct reprogramming. Cell Stem Cell *10*, 16–28.

Casis, O., Olesen, S.-P., and Sanguinetti, M.C. (2006). Mechanism of action of a novel human ether-a-go-go-related gene channel activator. Mol. Pharmacol. *69*, 658–665.

Caspi, O., Itzhaki, I., Kehat, I., Gepstein, A., Arbel, G., Huber, I., Satin, J., and Gepstein, L. (2009). In vitro electrophysiological drug testing using human embryonic stem cell derived cardiomyocytes. Stem Cells Dev. *18*, 161–172.

Clements, M., and Thomas, N. (2014). High-throughput multi-parameter profiling of electrophysiological drug effects in human embryonic stem cell derived cardiomyocytes using multi-electrode arrays. Toxicol. Sci. *140*, 445–461.

Eder, A., Hansen, A., Uebeler, J., Schulze, T., Neuber, C., Schaaf, S., Yuan, L., Christ, T., Vos, M.A., and Eschenhagen, T. (2014). Effects of proarrhythmic drugs on relaxation time and beating pattern in rat engineered heart tissue. Basic Res. Cardiol. *109*, 436.

Eschenhagen, T., Eder, A., Vollert, I., and Hansen, A. (2012). Physiological aspects of cardiac tissue engineering. Am. J. Physiol. Heart Circ. Physiol. *303*, H133–H143.

Feaster, T.K., Cadar, A.G., Wang, L., Williams, C.H., Chun, Y.W., Hempel, J.E., Bloodworth, N., Merryman, W.D., Lim, C.C., Wu, J.C., et al. (2015). Matrigel mattress: a method for the generation of single contracting human-induced pluripotent stem cell-derived cardiomyocytes. Circ. Res. *117*, 995–1000.

Fermini, B., Hancox, J.C., Abi-Gerges, N., Bridgland-Taylor, M., Chaudhary, K.W., Colatsky, T., Correll, K., Crumb, W., Damiano, B., Erdemli, G., et al. (2015). A new perspective in the field of cardiac safety testing through the comprehensive in vitro proarrhythmia assay paradigm. J. Biomol. Screen. *21*, 1–11.

Ferrantini, C., Coppini, R., Sacconi, L., Tosi, B., Zhang, M.L., Wang, G.L., de Vries, E., Hoppenbrouwers, E., Pavone, F., Cerbai, E., et al. (2014). Impact of detubulation on force and kinetics of cardiac muscle contraction. J. Gen. Physiol. *143*, 783–797.

Ferry, D.R., Glossmann, H., and Kaumann, A.J. (1985). Relationship between the stereoselective negative inotropic effects of verapamil enantiomers and their binding to putative calcium channels in human heart. Br. J. Pharmacol. *84*, 811–824.

Francis, G.S., Bartos, J.A., and Adatya, S. (2014). Inotropes. J. Am. Coll. Cardiol. *63*, 2069–2078.

Gómez, A.M., Valdivia, H.H., Cheng, H., Lederer, M.R., Santana, L.F., Cannell, M.B., McCune, S.A., Altschuld, R.A., and Lederer, W.J. (1997). Defective excitation-contraction coupling in experimental cardiac hypertrophy and heart failure. Science *276*, 800–806.

Guo, L., Coyle, L., Abrams, R.M.C., Kemper, R., Chiao, E.T., and Kolaja, K.L. (2013). Refining the human iPSC-cardiomyocyte arrhythmic risk assessment model. Toxicol. Sci. *136*, 581–594.

Hansen, A., Eder, A., Bönstrup, M., Flato, M., Mewe, M., Schaaf, S., Aksehirlioglu, B., Schwoerer, A.P., Uebeler, J., and Eschenhagen, T. (2010). Development of a drug screening platform based on engineered heart tissue. Circ. Res. *107*, 35–44.

Harris, K., Aylott, M., Cui, Y., Louttit, J.B., McMahon, N.C., and Sridhar, A. (2013). Comparison of electrophysiological data from human-induced pluripotent stem cell-derived cardiomyocytes to functional preclinical safety assays. Toxicol. Sci. *134*, 412–426.

Hirt, M.N., Sörensen, N.A., Bartholdt, L.M., Boeddinghaus, J., Schaaf, S., Eder, A., Vollert, I., Stöhr, A., Schulze, T., Witten, A., et al. (2012). Increased afterload induces pathological cardiac hypertrophy: a new in vitro model. Basic Res. Cardiol. *107*, 307.

Hirt, M.N., Hansen, A., and Eschenhagen, T. (2014). Cardiac tissue engineering: state of the art. Circ. Res. *114*, 354–367.

Hoekstra, M., Mummery, C.L., Wilde, A.A., Bezzina, C.R., and Verkerk, A.O. (2012). Induced pluripotent stem cell derived cardiomyocytes as models for cardiac arrhythmias. Front. Physiol. *3*, 346.

Ji, J., Kang, J., and Rampe, D. (2014). L-type Ca(2+) channel responses to Bay K 8644 in stem cell-derived cardiomyocytes are unusually dependent on holding potential and charge carrier. Assay Drug Dev. Technol. *12*, 352–360.

Jost, N., Virág, L., Bitay, M., Takács, J., Lengyel, C., Biliczki, P., Nagy, Z., Bogáts, G., Lathrop, D.A., Papp, J.G., et al. (2005). Restricting excessive cardiac action potential and QT prolongation: a vital role for IKs in human ventricular muscle. Circulation *112*, 1392–1399.

Joung, B., Tang, L., Maruyama, M., Han, S., Chen, Z., Stucky, M., Jones, L.R., Fishbein, M.C., Weiss, J.N., Chen, P.-S., et al. (2009). Intracellular calcium dynamics and acceleration of sinus rhythm by beta-adrenergic stimulation. Circulation *119*, 788–796.

Kang, J., Chen, X., Ji, J., Lei, Q., and Rampe, D. (2012). Ca^{2+} channel activators reveal differential L-type Ca^{2+} channel pharmacology between native and stem cell-derived cardiomyocytes. J. Pharmacol. Exp. Ther. *341*, 510–517.

Karakikes, I., Ameen, M., Termglinchan, V., and Wu, J.C. (2015). Human induced pluripotent stem cell-derived cardiomyocytes: insights into molecular, cellular, and functional phenotypes. Circ. Res. *117*, 80–88.

Kaufmann, S.G., Westenbroek, R.E., Maass, A.H., Lange, V., Renner, A., Wischmeyer, E., Bonz, A., Muck, J., Ertl, G., Catterall, W.A., et al. (2013). Distribution and function of sodium channel subtypes in human atrial myocardium. J. Mol. Cell. Cardiol. *61*, 133–141.

Kensah, G., Roa Lara, A., Dahlmann, J., Zweigerdt, R., Schwanke, K., Hegermann, J., Skvorc, D., Gawol, A., Azizian, A., Wagner, S., et al. (2013). Murine and human pluripotent stem cell-derived

cardiac bodies form contractile myocardial tissue in vitro. Eur. Heart J. *34*, 1134–1146.

Kramer, J., Obejero-Paz, C.A., Myatt, G., Kuryshev, Y.A., Bruening-Wright, A., Verducci, J.S., and Brown, A.M. (2013). MICE models: superior to the HERG model in predicting Torsade de Pointes. Sci. Rep. *3*, 2100.

Kuppusamy, K.T., Jones, D.C., Sperber, H., Madan, A., Fischer, K.A., Rodriguez, M.L., Pabon, L., Zhu, W.-Z., Tulloch, N.L., Yang, X., et al. (2015). Let-7 family of microRNA is required for maturation and adult-like metabolism in stem cell-derived cardiomyocytes. Proc. Natl. Acad. Sci. USA *112*, E2785–E2794.

Lakatta, E.G., Maltsev, V.A., and Vinogradova, T.M. (2010). A coupled SYSTEM of intracellular Ca^{2+} clocks and surface membrane voltage clocks controls the timekeeping mechanism of the heart's pacemaker. Circ. Res. *106*, 659–673.

Lee, P., Klos, M., Bollensdorff, C., Hou, L., Ewart, P., Kamp, T.J., Zhang, J., Bizy, A., Guerrero-Serna, G., Kohl, P., et al. (2012). Simultaneous voltage and calcium mapping of genetically purified human induced pluripotent stem cell-derived cardiac myocyte monolayers. Circ. Res. *110*, 1556–1563.

Lopez-Izquierdo, A., Warren, M., Riedel, M., Cho, S., Lai, S., Lux, R.L., Spitzer, K.W., Benjamin, I.J., Tristani-Firouzi, M., and Jou, C.J. (2014). A near-infrared fluorescent voltage-sensitive dye allows for moderate-throughput electrophysiological analyses of human induced pluripotent stem cell-derived cardiomyocytes. Am. J. Physiol. Heart Circ. Physiol. *307*, H1370–H1377.

Lundy, S.D., Zhu, W.-Z., Regnier, M., and Laflamme, M.A. (2013). Structural and functional maturation of cardiomyocytes derived from human pluripotent stem cells. Stem Cells Dev. *22*, 1991–2002.

Ma, J., Guo, L., Fiene, S.J., Anson, B.D., Thomson, J.A., Kamp, T.J., Kolaja, K.L., Swanson, B.J., and January, C.T. (2011). High purity human-induced pluripotent stem cell-derived cardiomyocytes: electrophysiological properties of action potentials and ionic currents. Am. J. Physiol. Heart Circ. Physiol. *301*, H2006–H2017.

Mesirca, P., Alig, J., Torrente, A.G., Müller, J.C., Marger, L., Rollin, A., Marquilly, C., Vincent, A., Dubel, S., Bidaud, I., et al. (2014). Cardiac arrhythmia induced by genetic silencing of "funny" (f) channels is rescued by GIRK4 inactivation. Nat. Commun. *5*, 4664.

Moretti, A., Laugwitz, K.-L., Dorn, T., Sinnecker, D., and Mummery, C. (2013). Pluripotent stem cell models of human heart disease. Cold Spring Harb. Perspect. Med. *3*, a014027.

Naito, H., Melnychenko, I., Didié, M., Schneiderbanger, K., Schubert, P., Rosenkranz, S., Eschenhagen, T., and Zimmermann, W.-H. (2006). Optimizing engineered heart tissue for therapeutic applications as surrogate heart muscle. Circulation *114*, I72–I78.

Navarrete, E.G., Liang, P., Lan, F., Sanchez-Freire, V., Simmons, C., Gong, T., Sharma, A., Burridge, P.W., Patlolla, B., Lee, A.S., et al. (2013). Screening drug-induced arrhythmia events using human induced pluripotent stem cell-derived cardiomyocytes and low-impedance microelectrode arrays. Circulation *128*, S3–S13.

Nishimura, S., Yasuda, S., Katoh, M., Yamada, K.P., Yamashita, H., Saeki, Y., Sunagawa, K., Nagai, R., Hisada, T., and Sugiura, S. (2004). Single cell mechanics of rat cardiomyocytes under isometric, unloaded, and physiologically loaded conditions. Am. J. Physiol. Heart Circ. Physiol. *287*, H196–H202.

Nunes, S.S., Miklas, J.W., Liu, J., Aschar-Sobbi, R., Xiao, Y., Zhang, B., Jiang, J., Massé, S., Gagliardi, M., Hsieh, A., et al. (2013). Biowire: a platform for maturation of human pluripotent stem cell-derived cardiomyocytes. Nat. Methods *10*, 781–787.

Okada, J.-I., Yoshinaga, T., Kurokawa, J., Washio, T., Furukawa, T., Sawada, K., Sugiura, S., and Hisada, T. (2015). Screening system for drug-induced arrhythmogenic risk combining a patch clamp and heart simulator. Sci. Adv. *1*, e1400142.

Oliveira, J.S., Redaelli, E., Zaharenko, A.J., Cassulini, R.R., Konno, K., Pimenta, D.C., Freitas, J.C., Clare, J.J., and Wanke, E. (2004). Binding specificity of sea anemone toxins to Nav 1.1-1.6 sodium channels. Unexpected contributions from differences in the IV/S3-S4 outer loop. J. Biol. Chem. *279*, 33323–33335.

Pointon, A., Harmer, A.R., Dale, I.L., Abi-Gerges, N., Bowes, J., Pollard, C., and Garside, H. (2015). Assessment of cardiomyocyte contraction in human-induced pluripotent stem cell-derived cardiomyocytes. Toxicol. Sci. *144*, 227–237.

Qu, Y., and Vargas, H.M. (2015). Proarrhythmia risk assessment in human induced pluripotent stem cell-derived cardiomyocytes using the maestro MEA platform. Toxicol. Sci. *147*, 286–295.

Redfern, W., Carlsson, L., Davis, A., Lynch, W., Mackenzie, I., Palethorpe, S., Siegl, P., Strang, I., Sullivan, A., and Wallis, R. (2003). Relationships between preclinical cardiac electrophysiology, clinical QT interval prolongation and torsade de pointes for a broad range of drugs: evidence for a provisional safety margin in drug development. Cardiovasc. Res. *58*, 32–45.

Riedel, M., Jou, C.J., Lai, S., Lux, R.L., Moreno, A.P., Spitzer, K.W., Christians, E., Tristani-Firouzi, M., and Benjamin, I.J. (2014). Functional and pharmacological analysis of cardiomyocytes differentiated from human peripheral blood mononuclear-derived pluripotent stem cells. Stem Cell Rep. *3*, 131–141.

Schaaf, S., Shibamiya, A., Mewe, M., Eder, A., Stöhr, A., Hirt, M.N., Rau, T., Zimmermann, W.-H., Conradi, L., Eschenhagen, T., et al. (2011). Human engineered heart tissue as a versatile tool in basic research and preclinical toxicology. PLoS One *6*, e26397.

Schaaf, S., Eder, A., Vollert, I., Stöhr, A., Hansen, A., and Eschenhagen, T. (2014). Generation of strip-format fibrin-based engineered heart tissue (EHT). Methods Mol. Biol. *1181*, 121–129.

Scott, C.W., Zhang, X., Abi-Gerges, N., Lamore, S.D., Abassi, Y.A., and Peters, M.F. (2014). An impedance-based cellular assay using human iPSC-derived cardiomyocytes to quantify modulators of cardiac contractility. Toxicol. Sci. *142*, 331–338.

Stieber, J., Herrmann, S., Feil, S., Löster, J., Feil, R., Biel, M., Hofmann, F., and Ludwig, A. (2003). The hyperpolarization-activated channel HCN4 is required for the generation of pacemaker action potentials in the embryonic heart. Proc. Natl. Acad. Sci. USA *100*, 15235–15240.

Sutko, J.L., and Willerson, J.T. (1980). Ryanodine alteration of the contractile state of rat ventricular myocardium. Comparison with dog, cat, and rabbit ventricular tissues. Circ. Res. *46*, 332–343.

Takahashi, K., Tanabe, K., Ohnuki, M., Narita, M., Ichisaka, T., Tomoda, K., and Yamanaka, S. (2007). Induction of pluripotent

stem cells from adult human fibroblasts by defined factors. Cell *131*, 861–872.

Thavandiran, N., Dubois, N., Mikryukov, A., Massé, S., Beca, B., Simmons, C.A., Deshpande, V.S., McGarry, J.P., Chen, C.S., Nanthakumar, K., et al. (2013). Design and formulation of functional pluripotent stem cell-derived cardiac microtissues. Proc. Natl. Acad. Sci. USA *110*, E4698–E4707.

Tulloch, N.L., Muskheli, V., Razumova, M.V., Korte, F.S., Regnier, M., Hauch, K.D., Pabon, L., Reinecke, H., and Murry, C.E. (2011). Growth of engineered human myocardium with mechanical loading and vascular coculture. Circ. Res. *109*, 47–59.

Wiegerinck, R.F., Cojoc, A., Zeidenweber, C.M., Ding, G., Shen, M., Joyner, R.W., Fernandez, J.D., Kanter, K.R., Kirshbom, P.M., Kogon, B.E., et al. (2009). Force frequency relationship of the human ventricle increases during early postnatal development. Pediatr. Res. *65*, 414–419.

Yang, X., Pabon, L., and Murry, C.E. (2014). Engineering adolescence: maturation of human pluripotent stem cell-derived cardiomyocytes. Circ. Res. *114*, 511–523.

Zhang, X.-H., Wei, H., Šarić, T., Hescheler, J., Cleemann, L., and Morad, M. (2015). Regionally diverse mitochondrial calcium signaling regulates spontaneous pacing in developing cardiomyocytes. Cell Calcium *57*, 321–336.

Zhou, Z., Gong, Q., Ye, B., Fan, Z., Makielski, J.C., Robertson, G.A., and January, C.T. (1998). Properties of HERG channels stably expressed in HEK 293 cells studied at physiological temperature. Biophys. J. *74*, 230–241.

Stem Cell Reports, Volume *7*

Supplemental Information

Human Engineered Heart Tissue: Analysis of Contractile Force

Ingra Mannhardt, Kaja Breckwoldt, David Letuffe-Brenière, Sebastian Schaaf, Herbert Schulz, Christiane Neuber, Anika Benzin, Tessa Werner, Alexandra Eder, Thomas Schulze, Birgit Klampe, Torsten Christ, Marc N. Hirt, Norbert Huebner, Alessandra Moretti, Thomas Eschenhagen, and Arne Hansen

Supplemental Information

Supplemental Data

Figure S1. Related to Figure 1.

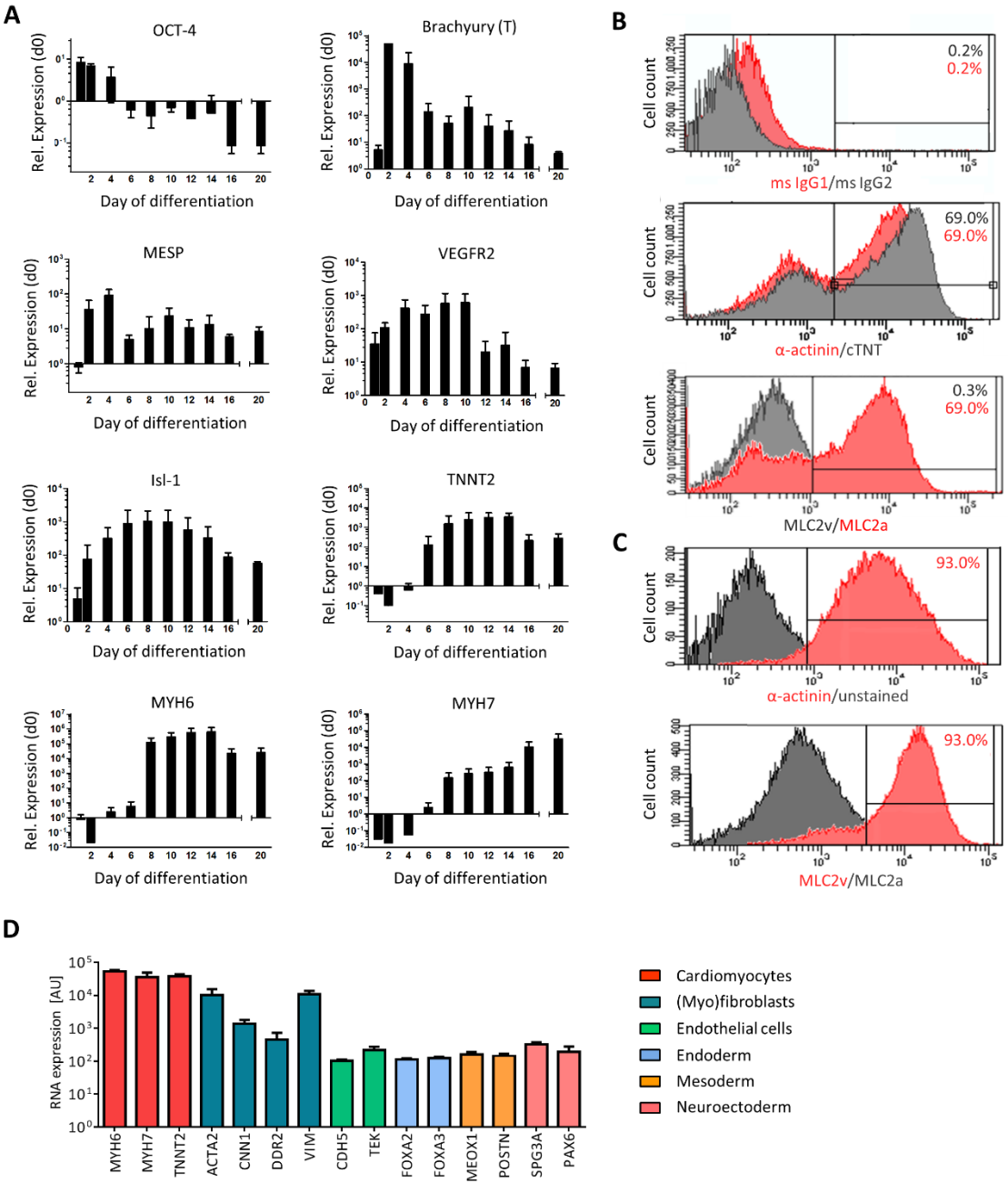

Figure S1: Cardiac differentiation. Replicates are indicated as "EHTs/number of independent experiments", depicted are mean±SEM. **A:** Quantitative RT-PCR results showing the relative expression levels of markers of pluripotency, mesoderm, early and late CM development over 20 days of differentiation (n=4/4). Expression levels are normalized to GUSB and expression levels at day 0. **B, C:** Characterization of differentiated cells by FACS analysis. **B:** Cells at the end of differentiation. **C:** Cells isolated from EHT after three weeks in culture. **D:** Characterization of cellular markers at the end (day 21) of differentiation. Relative RNA expression from whole transcriptome analysis for markers of cardiomyocytes, (myo)fibroblasts, endothelial cells, mesoderm, endoderm and neuroectoderm (n=4/1).

Figure S2. Related to Figure 2.

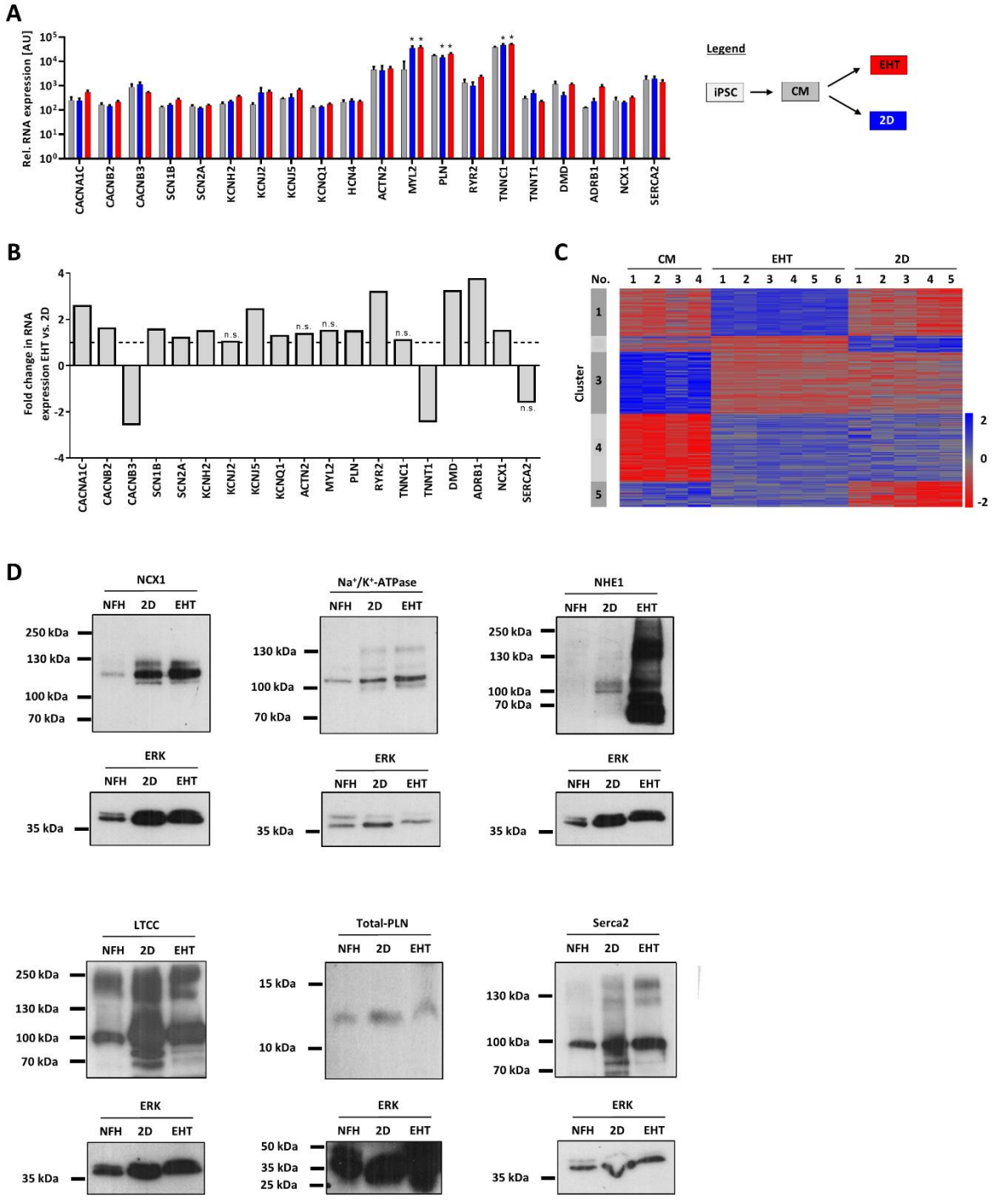

Figure S2: Expression analyses. Replicates are indicated as "EHTs/number of independent experiments". **A-D:** Gene and protein expression analysis comparing cardiomyocytes at the end of differentiation (CM; grey) with those cultivated for 21 more days in 2D (blue) or EHT (red) format (see legend). **A:** Gene expression levels comparing CM, 2D and EHT (Two-way ANOVA with Bonferroni's post-test; * $p<0.05$ vs. CM; n=4,5,6/3 for CM, 2D, EHT; depicted are mean±SEM). See also Table S1. **B:** Mean fold change in RNA expression in EHT (n=5/3) vs. 2D (n=6/3) for ion channels and cardiac genes. **C:** K-mean cluster analysis. See also Table S2 for functional aspects. **D:** Protein abundance of calcium handling proteins in 2D, EHT and non-failing human heart samples (NFH). Western blot analysis revealed expression of Na^+/Ca^{2+} exchanger-1 (NCX1, ~120 kDa), Na^+/K^+-ATPase (~112 kDa), Na^+/H^+ exchanger-1 (NHE1; ~100 kDa with an additional band at ~72 kDa 110-130 (glycosylated), 90 kDa (precursor), 210 kDa dimer), L-type calcium channel (~210 kDa), phospholamban (Total-PLN, ~12 kDa) and Serca2 ATPase (SERCA2, ~110 kDa). ERK (~40 kDa) was used as loading control.

Figure S3. Related to Figure 3.

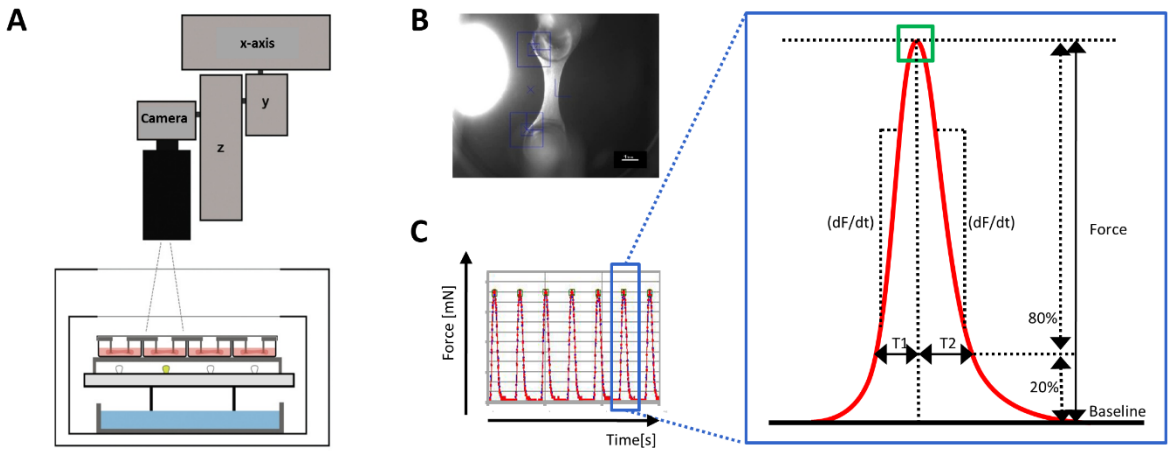

Figure S3: Contraction analysis of human EHTs. **A:** Setup with gas- and temperature-controlled incubation chamber with LEDs, glass top and camera above (adapted from Schaaf et al. 2011). **B:** Live-image of an EHT with depicted figure recognition (blue crosses) during the measurement. **C:** Force-time-diagram showing contraction peaks with contraction time (T1) and relaxation time (T2) at 20% peak height, contraction velocity (dF/dt), relaxation velocity (dF/dt) and force (green square as quality control for contraction peak identification of customized software).

Figure S4. Related to Figure 4.

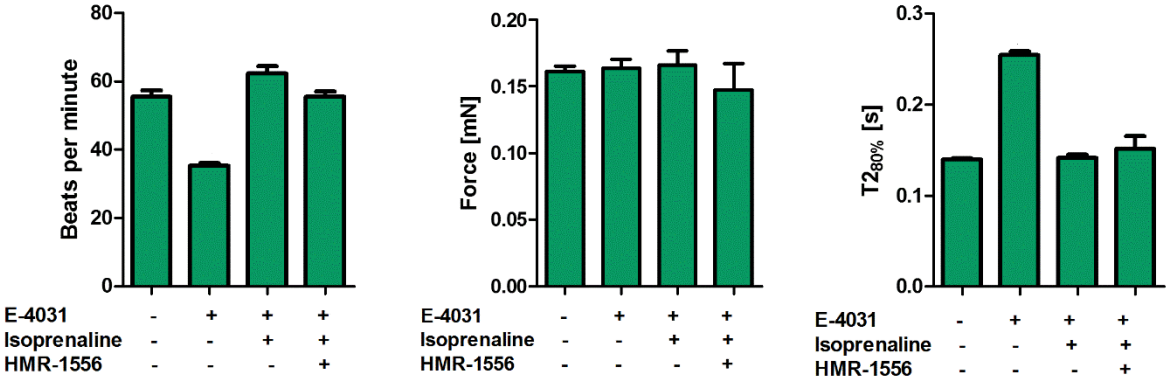

Figure S4: **I_{Ks}.** Response of spontaneous hiPSC-EHT contractions to I_{Ks}-inhibitor HMR-1556 (1 µM) after I_{Kr}-inhibition with E-4031 (100 nM) and ß-adrenergic stimulation with isoprenaline (10 nM). Change in beating frequency, contraction force and relaxation time T2 in modified Tyrode's solution with 1 mM calcium. Replicates are indicated as "EHTs/number of independent experiments"; n=4/1, depicted are mean±SEM.

Figure S5. Related to Figure 3 and Figure 5.

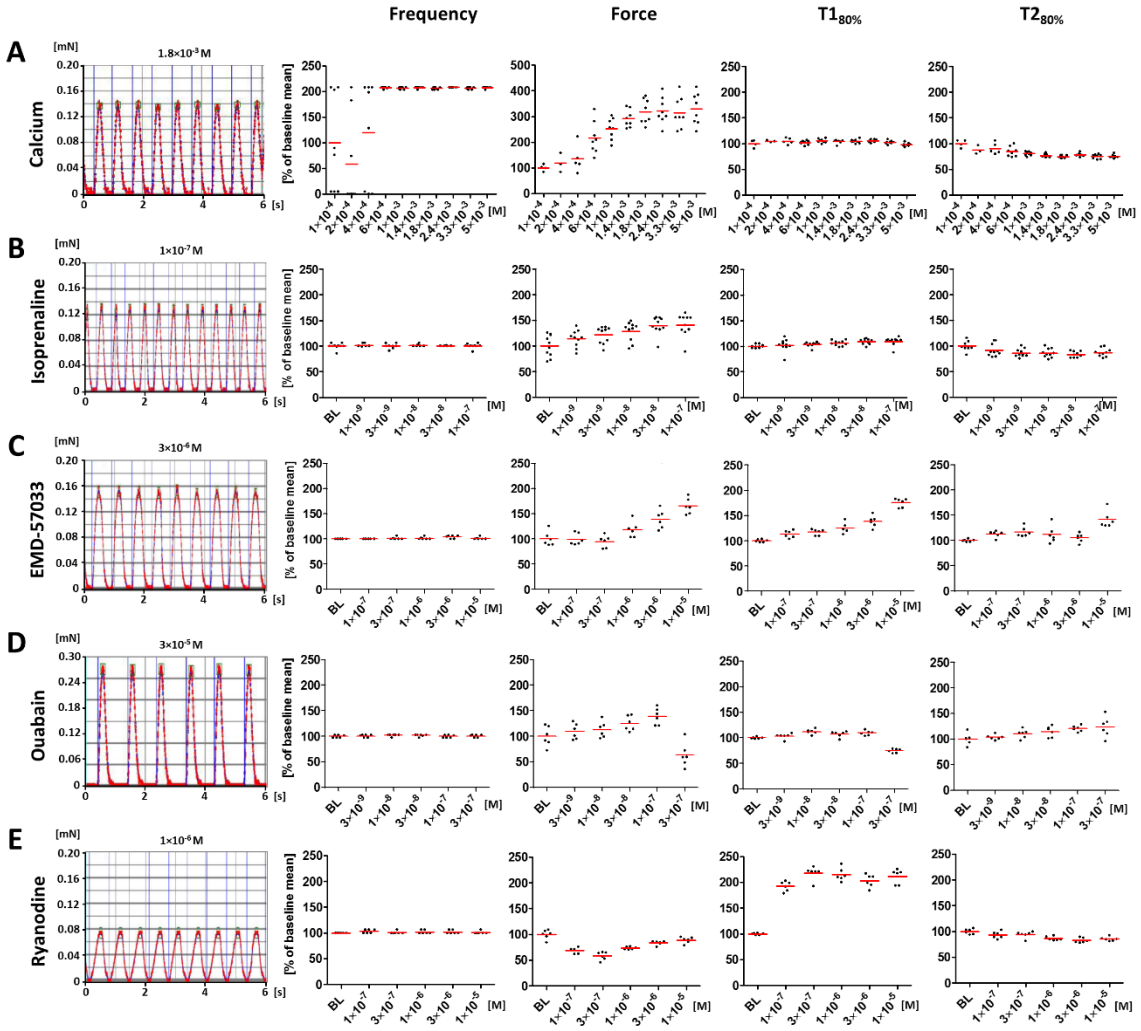

F

	hiPSC-EHT	NFH
Isoprenaline	+41% (peak force)	+300 – 800% (peak force) (Schotten et al. 2001, Böhm et al. 1991)
Calcium concentration response curve	EC_{50} 0.6 mM	EC_{50} of 5.6 mM (Böhm et al. 1991)
Calcium concentration response curve (skinned preparations)	EC_{50} of 2.4 µM (Stoehr et al. 2014)	EC_{50} of 1.06 µM (Hajjar & Gwathmey 1992)
Post-rest-potentiation	+17%	+76% (Pieske et al. 1996)
Frequency-dependent acceleration of relaxation	-14% (1-2 Hz)	-33% (1-2 Hz) (Mulieri et al. 1992)
Force-frequency-relationship	-/-	+68% (Pieske et al. 1996)
Frank-Starling law	+57%	+200% (Schwinger et al. 1994)

Figure S5: Pharmacological characterization of hiPSC-EHTs. A-E: Concentration response curves in modified Tyrode's solution (0.5-0.6 mM Ca^{2+}). Electrical stimulation: 1-2 Hz (blue lines). **Left:** Exemplary original recording of EHT contraction pattern at the indicated concentration. **Right:** Scatter-plot depiction of the concentration-response curve for frequency, force, contraction time (T1) and relaxation time (T2). Replicates are indicated as "EHTs/number of independent experiments"; n=6-10/1-2; data are depicted as scatter plot with mean. **F:** Comparison of effects in hiPSC-EHTs with published values in non-failing heart (NFH) tissue.

Figure S6. Related to Figure 6.

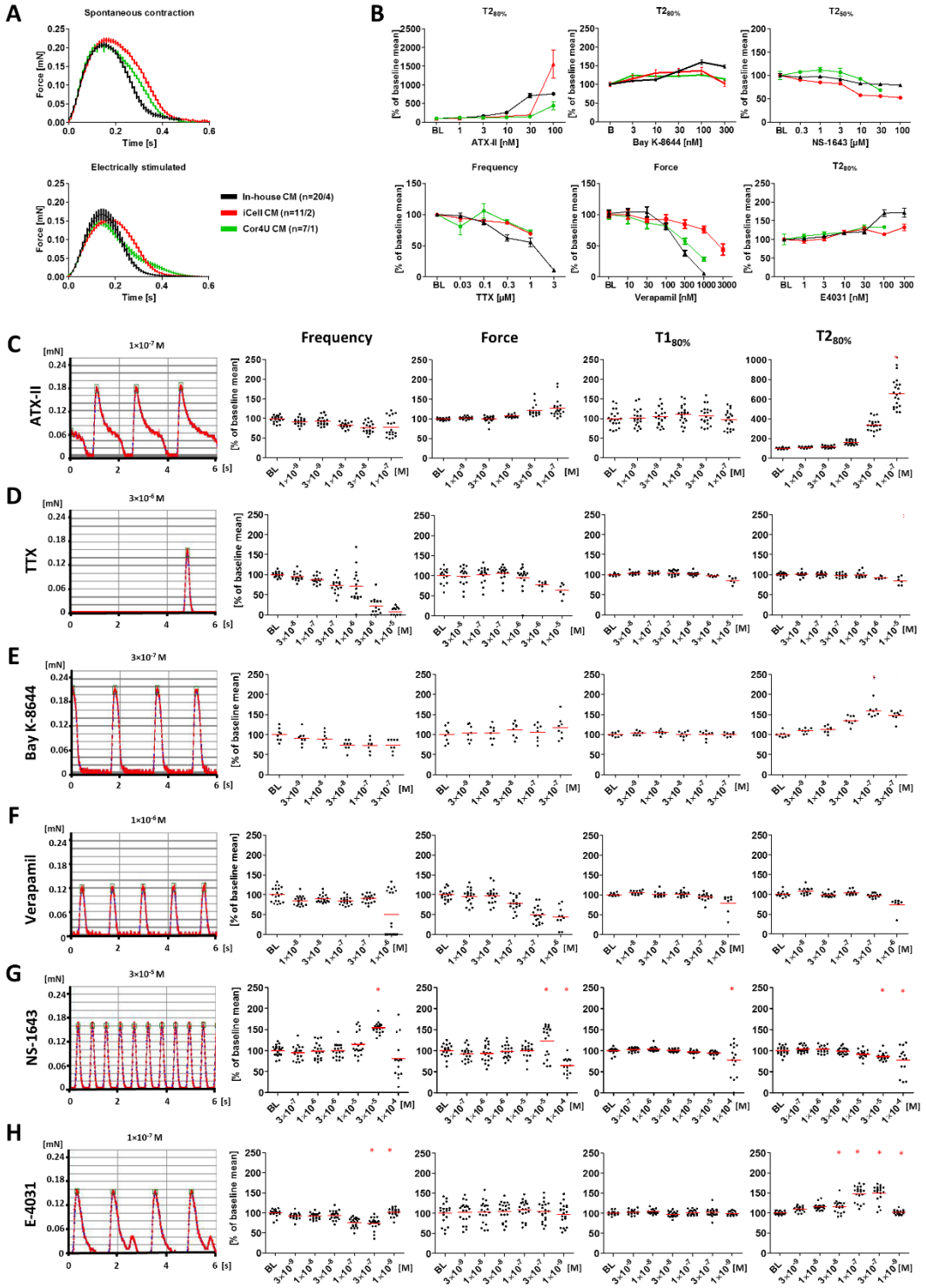

Figure S6: Pharmacological characterization of hiPSC-EHTs. **A:** Average contraction peaks (mean±SEM) of spontaneous contracting (top) and electrically stimulated (1.5 Hz; bottom) EHTs. Black: in-house reference CM (n=20/3), red: iCell® CM (n=11/2), green: Cor4U® CM (n=7/1), depicted are mean±SEM. **B:** Concentration response curves in modified Tyrode's solution (1.8 mM Ca^{2+}) for the ion channel modulators introduced in Figure 6 and their effect on the most prominently changed parameter of EHT contraction; depicted are mean±SEM. **C-H:** Concentration response curves in modified Tyrode's solution (1.8 mM Ca^{2+}) as partially displayed in Figure 6. **Left:** Exemplary original recording of EHT contraction pattern at the indicated concentration. **Right:** Scatter-plot depiction of the concentration-response curve for frequency, force, contraction time (T1) and relaxation time (T2). Replicates are indicated as "EHTs/number of independent experiments; n=8-20/2-3; data are depicted as scatter plot with mean. Statistical analysis for experiments with ≥3 independent experiments: One-way ANOVA with Dunnett's post-test vs. baseline conditions (BL); *p<0.05.

Figure S7. Related to Figure 3 and Figure 7.

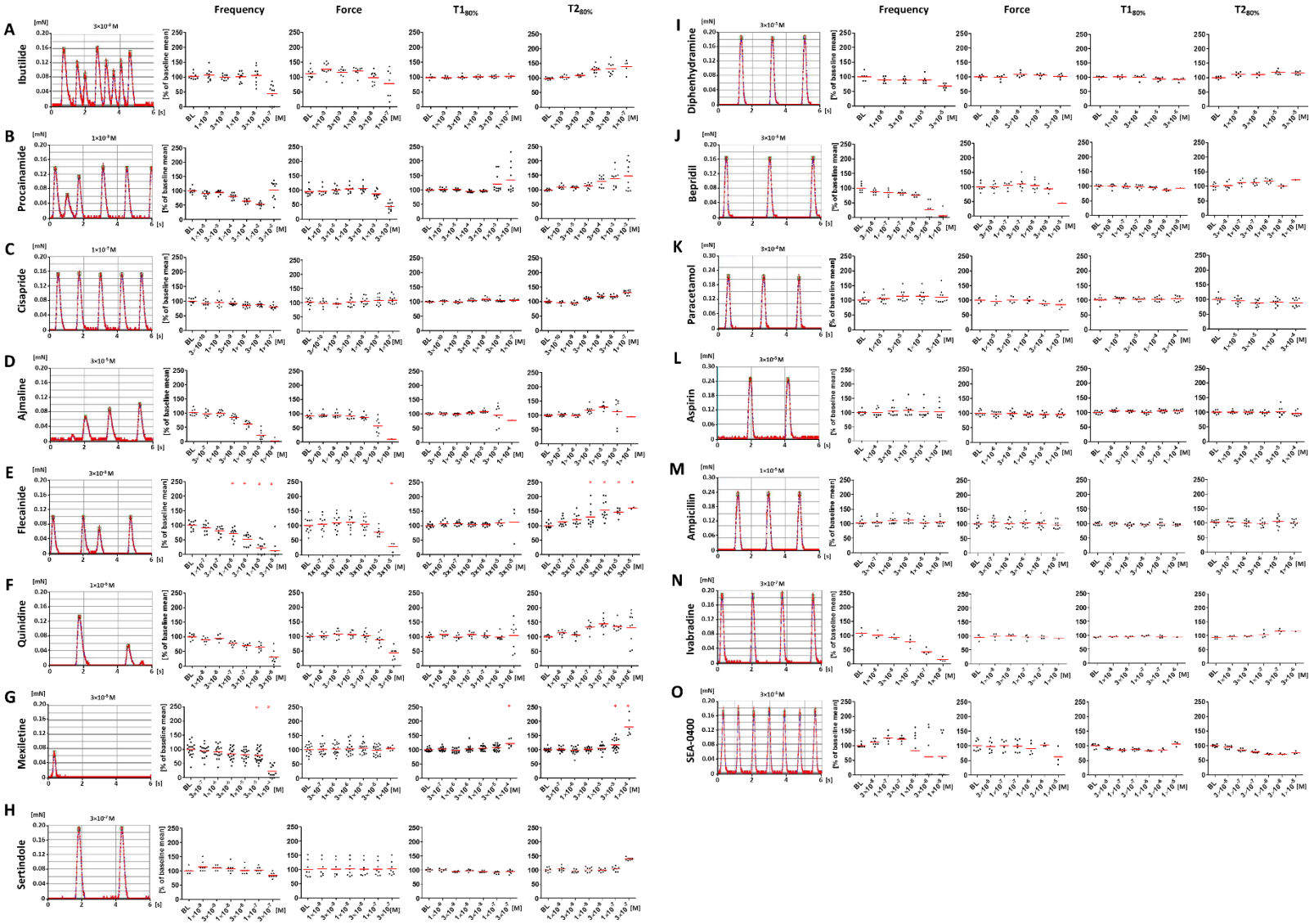

Figure S7: Pharmacological characterization of hiPSC-EHTs. Concentration response curves in modified Tyrode's solution (**A-N:** 1.8 mM Ca^{2+}, **O:** 1 mM Ca^{2+}). **Left:** Exemplary original recording of EHT contraction pattern at the indicated concentration. **Right:** Scatter-plot depiction of the concentration-response curve for frequency, force, contraction time (T1) and relaxation time (T2). Replicates are indicated as "EHTs/number of independent experiments"; n=4-23/1-3; data are depicted as scatter plot with mean. Statistical analysis for experiments with ≥3 independent experiments: One-way ANOVA with Dunnett's post-test vs. baseline conditions (BL); *p<0.05.

Table S1 (see external excel file). Related to Figure 2 and Figure S2.
Results of transcriptome analysis comparing CM with 21-days older time matched 2D and EHT culture.

Table S2. Related to Figure 2, Figure S2 and Table S1.
Enrichment analysis using G:Profiler, with a simulation based analytical threshold for significance estimation. BP = GeneOntology Biological Process; CC = GeneOntology Cellular Component; MF = GeneOntology Molecular Function; ke = KEGG database; mi = miRBase; tf = TransFac; a = annotation; q = query; inters. = intersection.

Source: Cluster 1 of 5: Genes differentially expressed in ANOVA (0.1% FDR; N=57)

p-value	Genes in annotation (a)	Genes in query (q)	a inters. q	(a inters. q) / q	(a inters. q) / a	Annotation-id	Database	Title
5.00e-02	1	10	1	0.100	1.000	OMIM:615219	omi	HYDROCEPHALUS, NONSYNDROMIC, AUTOSOMAL RECESSIVE 2; HYC2
5.00e-02	1	10	1	0.100	1.000	OMIM:201300	omi	NEUROPATHY, HEREDITARY SENSORY AND AUTONOMIC, TYPE IIA; HSAN2A;HSAN IIA;NEUROPATHY, HEREDITARY SENSORY, TYPE IIA; HSN2A;HSN IIA;ACROOSTEOLYSIS, NEUROGENIC;ACROOSTEOLYSIS, GIACCAI TYPE;NEUROPATHY, HEREDITARY SENSORY RADICULAR, AUTOSOMAL RECESSIVE;MORVAN DISEASE;NEUROPATHY, PROGRESSIVE SENSORY, OF CHILDREN;NEUROPATHY, CONGENITAL SENSORY
5.00e-02	1	10	1	0.100	1.000	OMIM:614492	omi	PSEUDOHYPOALDOSTERONISM, TYPE IIC; PHA2C
5.00e-02	1	10	1	0.100	1.000	OMIM:612313	omi	GLASS SYNDROME; GLASS;CHROMOSOME 2q32-q33 DELETION SYNDROME
5.00e-02	1	10	1	0.100	1.000	OMIM:615493	omi	MENTAL RETARDATION, AUTOSOMAL RECESSIVE 37; MRT37
5.00e-02	1	10	1	0.100	1.000	OMIM:614831	omi	SPINOCEREBELLAR ATAXIA, AUTOSOMAL RECESSIVE 13; SCAR13
5.00e-02	1	10	1	0.100	1.000	OMIM:258501	omi	3-@METHYLGLUTACONIC ACIDURIA, TYPE III; MGCA3;MGA, TYPE III; MGA3;OPTIC ATROPHY PLUS SYNDROME;OPTIC ATROPHY, INFANTILE, WITH CHOREA AND SPASTIC PARAPLEGIA;IRAQI-JEWISH 'OPTIC ATROPHY PLUS';COSTEFF SYNDROME;OPTIC ATROPHY 3, AUTOSOMAL RECESSIVE;OPA3, AUTOSOMAL RECESSIVE
5.00e-02	1	10	1	0.100	1.000	OMIM:165300	omi	OPTIC ATROPHY 3, AUTOSOMAL DOMINANT; OPA3;OPTIC ATROPHY AND CATARACT, AUTOSOMAL DOMINANT
5.00e-02	1	10	1	0.100	1.000	OMIM:607276	omi	RESTING HEART RATE, VARIATION IN;RHR

Source: Cluster 2 of 5: Genes differentially expressed in ANOVA (0.1% FDR; N=20)

p-value	Genes in annotation (a)	Genes in query (q)	a inters. q	(a inters. q) / q	(a inters. q) / a	Annotation-id	Database	Title
5.00e-02	1	2	1	0.500	1.000	CORUM:2003	cor	COX1 HOMODIMER COMPLEX

Source: Cluster 3 of 5: Genes differentially expressed in ANOVA (0.1% FDR; N=68)

p-value	Genes in annotation (a)	Genes in query (q)	a inters. q	(a inters. q) / q	(a inters. q) / a	Annotation-id	Database	Title
5.83e-05	181	51	8	0.157	0.044	GO:0035966	BP	RESPONSE TO TOPOLOGICALLY INCORRECT PROTEIN
3.57e-05	170	51	8	0.157	0.047	GO:0006986	BP	RESPONSE TO UNFOLDED PROTEIN
9.19e-04	259	51	8	0.157	0.031	GO:0034976	BP	RESPONSE TO ENDOPLASMIC RETICULUM STRESS
8.19e-06	141	51	8	0.157	0.057	GO:0035967	BP	CELLULAR RESPONSE TO TOPOLOGICALLY INCORRECT PROTEIN
4.85e-06	132	51	8	0.157	0.061	GO:0034620	BP	CELLULAR RESPONSE TO UNFOLDED PROTEIN
4.04e-06	129	51	8	0.157	0.062	GO:0030968	BP	ENDOPLASMIC RETICULUM UNFOLDED PROTEIN RESPONSE
3.98e-02	19	51	3	0.059	0.158	GO:0036499	BP	PERK-MEDIATED UNFOLDED PROTEIN RESPONSE
1.33e-02	169	24	5	0.208	0.030	KEGG:04141	keg	PROTEIN PROCESSING IN ENDOPLASMIC RETICULUM
2.57e-02	532	48	8	0.167	0.015	MI:hsa-miR-130a*	mi	MI:HSA-miR-130a*
4.12e-04	87	21	5	0.238	0.057	REAC:381119	rea	UNFOLDED PROTEIN RESPONSE (UPR)
9.69e-03	28	21	3	0.143	0.107	REAC:381042	rea	PERK REGULATES GENE EXPRESSION
4.00e-02	10054	54	38	0.704	0.004	TF:M00932_1	tf	FACTOR: SP1; MOTIF: NNGGGGCGGGGNN; MATCH CLASS: 1
3.05e-02	11319	54	41	0.759	0.004	TF:M07354_0	tf	FACTOR: EGR-1; MOTIF: GCGGGGGCGG; MATCH CLASS: 0
4.56e-02	5051	54	25	0.463	0.005	TF:M03567_1	tf	FACTOR: SP2; MOTIF: NYSGCCCCGCCCCCY; MATCH CLASS: 1

Source: Cluster 4 of 5: Genes differentially expressed in ANOVA (0.1% FDR; N=82)

p-value	Genes in annotation (a)	Genes in query (q)	a inters. q	(a inters. q) / q	(a inters. q) / a	Annotation-id	Database	Title
4.27e-02	6363	78	38	0.487	0.006	TF:M01072_1	tf	FACTOR: HIC1; MOTIF: NSNNNNTGCCCSSNN; MATCH CLASS: 1

Source: Cluster 5 of 5: Genes differentially expressed in ANOVA (0.1% FDR; N=32)

p-value	Genes in annotation (a)	Genes in query (q)	a inters. q	(a inters. q) / q	(a inters. q) / a	Annotation-id	Database	Title
5.00e-02	1	2	1	0.500	1.000	OMIM:300376	omi	MUSCULAR DYSTROPHY, BECKER TYPE; BMD;BECKER MUSCULAR DYSTROPHY;MUSCULAR DYSTROPHY, PSEUDOHYPERTROPHIC PROGRESSIVE, BECKER TYPE
5.00e-02	1	2	1	0.500	1.000	OMIM:613152	omi	MUSCULAR DYSTROPHY-DYSTROGLYCANOPATHY (CONGENITAL WITHOUT MENTAL RETARDATION),TYPE B, 4; MDDGB4;MUSCULAR DYSTROPHY, CONGENITAL, FKTN-RELATED
5.00e-02	1	2	1	0.500	1.000	OMIM:302045	omi	CARDIOMYOPATHY, DILATED, 3B; CMD3B;CARDIOMYOPATHY, DILATED, X-LINKED; XLCM
5.00e-02	1	2	1	0.500	1.000	OMIM:253800	omi	MUSCULAR DYSTROPHY-DYSTROGLYCANOPATHY (CONGENITAL WITH BRAIN AND EYEANOMALIES), TYPE A, 4; MDDGA4;FUKUYAMA CONGENITAL MUSCULAR DYSTROPHY; FCMD;WALKER-WARBURG SYNDROME OR MUSCLE-EYE-BRAIN DISEASE, FKTN-RELATED
5.00e-02	1	2	1	0.500	1.000	OMIM:611615	omi	CARDIOMYOPATHY, DILATED, 1X; CMD1X;CARDIOMYOPATHY, DILATED, WITH MILD OR NO PROXIMAL MUSCLE WEAKNESS
5.00e-02	1	2	1	0.500	1.000	OMIM:611588	omi	MUSCULAR DYSTROPHY-DYSTROGLYCANOPATHY (LIMB-GIRDLE), TYPE C, 4; MDDGC4;MUSCULAR DYSTROPHY, LIMB-GIRDLE, TYPE 2M; LGMD2M
5.00e-02	1	2	1	0.500	1.000	OMIM:310200	omi	MUSCULAR DYSTROPHY, DUCHENNE TYPE; DMD;DUCHENNE MUSCULAR DYSTROPHY;MUSCULAR DYSTROPHY, PSEUDOHYPERTROPHIC PROGRESSIVE, DUCHENNE TYPE

Supplemental Experimental Procedures

Expansion and differentiation of human induced pluripotent stem cells

Undifferentiated hiPSC control cell line (Moretti et al. 2010; in the following named "in-house reference") was expanded on Geltrex® (Gibco, A1413302; 1:200 in DMEM, 37 °C, 30 min) coated 6-well-dishes and T80-flasks in FTDA medium (37 °C, 5% CO_2, 5% O_2) as recently published (Frank et al., 2012) with 30 ng/ml FGF2: DMEM/F-12 (Gibco, 21331), 2 mM L-Glutamine (Gibco, 25030), 0.5% penicillin/streptomycin (Gibco, 15140), 5 mg/l transferrin (Sigma, T8158), 5 µg/l selenium (Sigma, S5261), 0.1% human serum albumin (Biopur, 05-720-1B), 1x Lipid-Mix (Sigma-Aldrich, L5146), 5 mg/l insulin (Sigma-Aldrich, I9278), 50 nM dorsomorphin (Tocris, 3093), 2.5 ng/ml activin A (R&D Systems, 338-AC), 0.5 ng/ml human TGFß1 (PeproTech, 100-21C), 30 ng/ml FGF2 (PeproTech, 100-18B). Cardiomyocytes were differentiated from hiPSC in a three-stage protocol (Figure 1). Confluent hiPSC were incubated with Rho kinase inhibitor Y-27632 (Biaffin, PKI-Y27632-010; 10 µM in FTDA medium) for 1 hour, washed with PBS (Gibco, 14190) twice and dissociated with 0.5 mM EDTA (10 minutes; Roth, 80432). After automated cell counting (CASY® cell counter, OMNI Life Science), cells were transferred to spinner flasks. Embryoid bodies (EBs) were generated during culture of single cell suspension (30×10^6 cells/100 ml) in 250 and 500 ml spinner flasks (FTDA medium with 4 mg/ml polyvinyl alcohol [PVA; Sigma-Aldrich, P8136], 10 µM Y-27632) by stirring at 40 rpm in a gas and temperature controlled incubator (37 °C, 5% CO_2, 5% O_2) for 24 h (Zweigerdt et al., 2011). An aliquot of EBs was transferred into a 15 ml falcon tube and EBs were sedimented (10 min). EB volume of the aliquot was estimated according to falcon tube scale and EB volume of the entire preparation was calculated. Mesodermal differentiation was induced in suspension culture on Pluronic® F-127 (Sigma-Aldrich, P2443; 1% in PBS, 37 °C, overnight) coated T175 flasks (200 µl EBs/40 ml medium) for three days with daily medium change of 50% of the volume (37 °C, 5% CO_2, 5% O_2). The medium consisted of RPMI 1640 (Gibco, 21875), 4 mg/ml PVA, 0.5% penicillin/streptomycin, 10 mM HEPES (pH 7.4; Roth, 9105.4), 0.05% human serum albumin, 5 mg/l transferrin, 5 µg/l selenium, 10 µM Y-27632, 0.1% Lipid-Mix, 250 µM 2-phospho-L-ascorbic acid trisodium salt (Sigma-Aldrich, 49752), 10 ng/ml BMP-4 (R&D Systems, 314-BP), 3 ng/ml activin-A, 5 ng/ml FGF2. Cardiac differentiation was performed either in suspension culture or in adhesion culture (Figure 1) with a medium consisting of RPMI 1640, 0.5% penicillin/streptomycin, 10 mM HEPES, 1% transferrin-selenium, 1 µM Y-27632, 0.05% Lipid-Mix, 250 µM 2-phospho-L-ascorbic acid trisodium salt, 0.1% human serum albumin, 100 nM Wnt-inhibitor DS-07 (4-(*cis-endo*-1,3-dioxooctahydro-*2H*-4,7-methanoisoindol-2-yl)-*N*-(quinolin-8-yl)-*trans*-cyclo-hexylcarboxamide; (Lanier et al., 2012); 37 °C, 5% CO_2, 21% O_2). For adhesion culture EBs were transferred to Geltrex® coated vessels and evenly distributed (100 µl EBs/T75 flask). For suspension culture the EBs were left in the Pluronic® coated vessels. The attached or suspended colonies were cultured for three days with medium change only on day 2 and 3. For the next four days the cells were cultured in RPMI 1640 supplemented with 0.5% penicillin/streptomycin, 10 mM HEPES, 500 µM 1-thioglycerol (Sigma, M6145), 1 µM Y-27632, 2% B-27 supplement (Gibco, 17504-044), 100 nM DS-07 (37 °C, 5% CO_2, 21% O_2). Spontaneous beating usually occurred around day 9-11 of cardiac differentiation. For the following 4-5 days the beating colonies were cultured in the same medium composition without the addition of the WNT-inhibitor DS-07.

Flow cytometry (FACS) analysis

HiPSC-cardiomyocytes were dissociated to single-cell suspensions with collagenase 2 (200 U/ml, Worthington, LS004176 in HBSS minus Ca^{2+}/Mg^{2+}, Gibco, 14175-053) for 4 h at 37 °C. Cells were fixed with ice-cold methanol for 20 min at 4 °C and the cell membrane permeabilized in FACS buffer containing 0.5% saponine. Intracellular proteins were stained successively with primary and secondary antibodies in FACS buffer containing 0.5% saponine for 30 min at 4 °C. The following antibodies were used: alpha-actinin (Sigma-Aldrich, A7811, 1:800), MLC2a (Synaptic Systems, 311011, 1:100), MLC2v (Proteintech, 10906-1-AP, 1:100), troponin T (Abcam, ab45932, 1:800), Alexa Fluor® 488 anti-rabbit (Life technologies, A-11034, 1:800), Alexa Fluor® 488 anti-mouse (Life technologies, A-11001, 1:800). For negative control we used isotype antibodies (Figure S1B): anti-mouse IgG1 for alpha-actinin and troponin T and anti-mouse IgG2b for MLC2a. Samples were analyzed with a BD FACSCanto II Flow Cytometer and the BD FACSDiva Software 6.0.

Quantitative PCR

Samples were taken on day 0, between day 2 and day 16 every other day and on day 20 of differentiation. For each time point, four differentiation runs were analysed. RNA was isolated after proteinase K digestion with the RNeasy Kit (Qiagen) according to manufacturer's instructions. The conversion to cDNA was performed with the High Capacity cDNA Reverse Transcription Kit (Applied Biosystems). QPCR was performed with SYBR-Green

(Fermentas) according to manufacturer's instructions in technical triplicates. Glucuronidase-beta (GUSB) was used as reference transcript for normalization. The target sequences were amplified during 40 cycles in an AbiPrism7000HT cycler.

Primer sequences (5´→ 3´):

Name	Gene	Primer (forward)	Primer (reverse)
Alpha MHC	MYH6	TTCATTGACTTTGGCATGGA	GGCTTCTGGAAATTGTTGGA
Beta MHC	MYH7	CACAGCTCTGTCCTGCTCTG	TTCTAGCCGCTCCTTCTCTG
Cardiac troponin T (total)	TNNT2	TTCGACCTGCAGGAGAAGTT	GAGCGAGGAGCAGATCTTTG
Glucoronidase beta	GUSB	AAACGATTGCAGGGTTTCAC	CTCTCGTCGGTGACTGTTCA
Brachyury homolog	T	GCAAAAGCTTTCCTTGATGC	ATGAGGATTTGCAGGTGGAC
Islet	ISL1	GTTACCAGCCACCTTGGAAA	GGACTGGCTACCATGCTGTT
Mesoderm posterior 1 homolog	MESP	GAAGTGGTTCCTTGGCAGAC	TCCTGCTTGCCTCAAAGTGT
Kinase insert domain receptor, VEGFR2	KDR/ FLK1	GCGATGGCCTCTTCTGTAAG	ACACGACTCCATGTTGGTCA
Oct4 POU class 5 homeobox 1	POU5F1	CGAAAGAGAAAGCGAACCAG	GCCGGTTACAGAACCACACT

Transcriptome analysis

For transcriptome analysis we isolated RNA from cardiomyocytes at the end of differentiation and matched cultures (21 days) of hiPSC-CM in either 2D or EHT format. Cells and EHTs were washed twice in PBS, EHTs stripped from the silicone racks, and homogenized by trituration through small steel cannulas (Braun Sterican; 21G then 27G) in lysis buffer (RNeasy® mini kit , Qiagen 74104) and digested with Proteinase K (Qiagen 19133; 56 °C, 10 min). RNA was isolated with the RNeasy® mini kit (Qiagen 74104) according to standard protocol. Array data (Illumina Human HT-12 v2) were processed on the Illumina GenomeStudio V2011.1 Platform (Gene Expression Module 1.9.0), two slides, five conditions with four to five biological replicates each (cardiomyocytes, n=4/3; cardiomyocytes 2D, n=5/3; cardiomyocytes EHT, n=6/3; NCBI GEO accession number GSE80390). The array data have been quantile normalized on probe level (47,310 probes) without background correction. Probes absent in all samples (minimum detection p-value >0.05) were rejected. The remaining set of 29,258 probes underwent parametric ANOVA statistic using Partek Genomic Suite 6.7 (Table S1). ANOVA was done by taking the batch differences into account. Multiple testing correction was performed using false discovery rate (FDR) statistic (Benjamini & Hochberg, 1995). Probes underwent 0.1% FDR (n=277) were further investigated with clustering and functional enrichment approaches. General differentiation of the cell-type specific expression profiles was performed using hierarchical clustering. The K-mean clustering with Euclidean distance function was done using standardized values. K=5 was selected according to the result of the Davies Bouldin K estimation procedure (data not shown here). Functional aspects of the differential expression was analyzed using the G:Profiler interface (Reimand et al., 2007) using g:SCS threshold as significance criterion.

Histological analysis

30-35 days old EHTs were fixed in formaldehyde (Roti®-Histofix 4%, Carl Roth, P087.3) overnight at 4 °C. After embedding in paraffin, 4 µm thick longitudinal or cross sections were processed for immunohistochemical staining (monoclonal mouse anti-MLC2v 1:200, Synaptic systems 310111; monoclonal mouse anti-dystrophin 1:200, Millipore MAB1645). For whole mount immunofluorescence staining, fixed EHTs were blocked (6 h in TBS 0.05 M pH 7.4, 10% FCS, 1% BSA, 0.5% Triton X-100), incubated in antibody solution (TBS 0.05 M pH 7.4, 1% BSA, 0.5% Triton X-100) with primary antibodies (monoclonal mouse anti-α-actinin 1:800, Sigma A7811; monoclonal

rabbit anti-MLC2v 1:200, Proteintec™, 10906-1-AP; polyclonal rabbit anti-caveolin-3 1:1000, Novus Biologicals NB110-5029; polyclonal rabbit anti-junctophilin-2 1:100, Santa Cruz sc-134875), washed repeatedly with PBS, incubated in antibody solution with secondary antibodies and other stainings (Alexa Fluor® 488 goat-anti-mouse 1:800, Invitrogen; Alexa Fluor® 488 goat-anti-rabbit 1:800, Invitrogen; Alexa Fluor® 546 goat-anti-rabbit 1:200; DRAQ5™ 1:1000, Biostatus Ltd. BOS-889-001-R050; Phalloidin Alexa Fluor® 488 1:60; Invitrogen A-12379), rinsed 3-4 times in PBS and embedded in Fluoromount-G® (SouthernBiotech, 0100-01) in dented microscope slides (Carl Roth, H884.1). 2D cultures were cultivated on coated (0.1% gelatin) glas cover slips and handled accordingly.

Transmission electron microscopy

For transmission electron microscopy (TEM), EHTs were washed twice in PBS and incubated in 2-butandionemonoxime (Sigma, B0753; 30 mM in PBS, 10 min, 37 °C) to relax sarcomeres and fixed overnight in glutaraldehyde (0.36%, pH 7.0-7.5, 4 °C). Fixed EHTs were removed from silicone racks and subjected to post-fixation in osmium tetroxide solution (1%, 2 h; Science Services, 19110), dehydration and embedding in a glycidether-based resin. Ultra-thin sections (50 nm) were prepared and analyzed on a Zeiss LEO 912AB.

Western blot

21 days old hiPSC-EHTs were frozen in liquid nitrogen and stored at -80 °C. 70 µl of 1x M-PER™ Mammalian Protein Extraction Reagent (Thermo Scientific) supplemented with protease and phosphatase inhibitor (Roche) was used for the lysis per EHT. Age-matched hiPSC-CM 2D cultures or samples of non-failing human heart (NFH) were handled accordingly. After homogenization, 1x Laemmli buffer was added to the samples before heating at 95 °C for 5 minutes. SDS polyacrylamide gels (8-15%) were loaded with 4 µl of NFH lysate, 10 µl of 2D lysate and 20 µl of EHT lysate per lane. After separation, proteins were blotted onto PVDF or nitrocellulose membranes using the wet blot method. Membranes were cut, blocked in 5-10% low fat milk powder solution in TBS-Tween 0.1% and incubated over night at 4 °C with primary antibodies against ERK (1:1000, mAB#4695/Cell Signaling), L-type calcium channel (1:100, ACC-013/Alomone), Na^+/Ca^{2+} exchanger-1 (1:500, ab6495/abcam), Na^+/K^+-ATPase (1:500, #05-369/Millipore), total phospholamban (1:5000, A010-14/Badrilla), Serca2 ATPase (1:1000, MA3-919/ Thermo Scientific), Na^+/H^+ exchanger-1 (1:500, sc-28758/SantaCruz). After washing, membranes were incubated either with anti-rabbit IgG peroxidase-conjugated secondary antibody (1:5000, A0545/Sigma) or with anti-mouse IgG peroxidase-conjugated secondary antibody (1:5000, A3682/Sigma) in 5% low fat milk powder solution in TBS-Tween 0.1% for one hour at room temperature. Pierce® ECL Western Blotting Substrate (Thermo Scientific) was used for the visualization of the bands (Figure S2).

Contractile analysis of human EHTs with increase in preload

Inotropic responses to increase in preload (Frank-Starling law) of hiPSC-EHTs were determined under electrical stimulation (1-2 Hz) and perfusion in a temperature controlled (37 °C) organ bath filled with Tyrode's solution (see above, without HEPES, plus 0.3 mM ascorbic acid). Data collection and evaluation were performed with a custom-made software (BMON, G. Jäckel, Hanau) as previously described (Zimmermann et al., 2000). Preload was increased in 40 µm intervals until the force reached a plateau.

Supplemental References

Benjamini, Y., and Hochberg, Y. (1995). Controlling the false discovery rate: a practical and powerful approach to multiple testing. J. Roy. Statist. Soc. Ser. *B 57*, 289-300.

Bohm, M., Morano, I., Pieske, B., Ruegg, J.C., Wankerl, M., Zimmermann, R., and Erdmann, E. (1991). Contribution of cAMP-phosphodiesterase inhibition and sensitization of the contractile proteins for calcium to the inotropic effect of pimobendan in the failing human myocardium. Circ Res *68*, 689–701.

Hajjar, R.J., and Gwathmey, J.K. (1992). Cross-bridge dynamics in human ventricular myocardium. Regulation of contractility in the failing heart. Circulation *86*, 1819–1826.

Moretti, A., Bellin, M., Welling, A., Jung, C.B., Lam, J.T., Bott-Flügel, L., Dorn, T., Goedel, A., Höhnke, C., Hofmann, F., et al. (2010). Patient-specific induced pluripotent stem-cell models for long-QT syndrome. N Engl J Med 363, 1397–1409.

Mulieri, L.A., Hasenfuss, G., Leavitt, B., Allen, P.D., and Alpert, N.R. (1992). Altered myocardial force-frequency relation in human heart failure. Circulation *85*, 1743–1750.

Pieske, B., Sütterlin, M., Schmidt-Schweda, S., Minami, K., Meyer, M., Olschewski, M., Holubarsch, C., Just, H., and Hasenfuss, G. (1996). Diminished post-rest potentiation of contractile force in human dilated cardiomyopathy: Functional evidence for alterations in intracellular Ca2+ handling. J Clin Invest *98*, 764–776.

Reimand, J., Kull, M., Peterson, H., Hansen, J., and Vilo, J. (2007). g:Profiler — a web-based toolset for functional profiling of gene lists from large-scale experiments. Nucleic Acids Res. *35*, W193-200.

Schotten, U., Ausma, J., Stellbrink, C., Sabatschus, I., Vogel, M., Frechen, D., Schoendube, F., Hanrath, P., and Allessie, M.A. (2001). Cellular mechanisms of depressed atrial contractility in patients with chronic atrial fibrillation. Circulation *103*, 691–698.

Schwinger, R.H., Böhm, M., Koch, A., Schmidt, U., Morano, I., Eissner, H.J., Uberfuhr, P., Reichart, B., and Erdmann, E. (1994). The failing human heart is unable to use the Frank-Starling mechanism. Circ Res *74*, 959–969.

Stoehr, A., Neuber, C., Baldauf, C., Vollert, I., Friedrich, F.W., Flenner, F., Carrier, L., Eder, A., Schaaf, S., Hirt, M.N., et al. (2014). Automated analysis of contractile force and Ca2+ transients in engineered heart tissue. Am J Physiol Heart Circ Physiol *306*, H1353–H1363.

Zimmermann, W.-H.H., Fink, C., Kralisch, D., Remmers, U., Weil, J., and Eschenhagen, T. (2000). Three-dimensional engineered heart tissue from neonatal rat cardiac myocytes. Biotechnol Bioeng 68, 106–114.